Economics Working Paper Series

2019/006

Time-Varying General Dynamic Factor Models and the Measurement of Financial Connectedness

Matteo Barigozzi, Marc Hallin and Stefano Soccorsi

The Department of Economics
Lancaster University Management School
Lancaster LA1 4YX
UK

LUMS home page: http://www.lancaster.ac.uk/lums/

Time-Varying General Dynamic Factor Models and the Measurement of Financial Connectedness

Matteo Barigozzi[1] Marc Hallin[2] Stefano Soccorsi[3]

4th February 2019

Abstract

Ripple effects in financial markets associated with crashes, systemic risk and contagion are characterized by non-trivial lead-lag dynamics which is crucial for understanding how crises spread and, therefore, central in risk management. In the spirit of Diebold and Yilmaz (2014), we investigate connectedness among financial firms via an analysis of impulse response functions of adjusted intraday log-ranges to market shocks involving network theory methods. Motivated by overwhelming evidence that the interdependence structure of financial markets is varying over time, we are basing that analysis on the so-called time-varying General Dynamic Factor Model proposed by Eichler et al. (2011), which extends to the locally stationary context the framework developed by Forni et al. (2000) under stationarity assumptions. The estimation methods in Eichler et al. (2011), however, present the major drawback of involving two-sided filters which make it impossible to recover impulse response functions. We therefore introduce a novel approach extending to the time-varying context the one-sided method of Forni et al. (2017). The resulting estimators of time-varying impulse response functions are shown to be consistent, hence can be used in the analysis of (time-varying) connectedness. Our empirical analysis on a large and strongly comoving panel of intraday price ranges of US stocks indicates that large increases in mid to long-run connectedness are associated with the main financial turmoils.

JEL subject classification: C32, C14.

Key words: Dynamic factor models, volatility, financial crises, contagion, financial connectedness, high-dimensional time series, panel data, time-varying models, local stationarity.

[1]m.barigozzi@lse.ac.uk – Department of Statistics, London School of Economics and Political Science, UK.
[2]mhallin@ulb.ac.be – ECARES, Université Libre de Bruxelles, Belgium.
[3]s.soccorsi@lancaster.ac.uk– Department of Economics, Lancaster University Management School, UK.

1 Introduction

Measuring financial risk is a long-standing challenge of paramount importance for risk management, portfolio optimization, business cycle analysis and, ultimately, financial regulation. Fostered by the recent global financial crisis, in the last few years an increasing number of approaches have been proposed to assess market fragility and its propensity to pervasively propagate amplified shocks and so overwhelm the financial system as a whole.

Even though, as reviewed by Benoit et al. (2017) *systemic risk* is a "hard-to-define-but-you-know-it-when-you-see-it" kind of thing, its quantitative analysis is essentially a measurement of comovements. Acharya et al. (2017), extending previous works of Acharya et al. (2012) and Brownlees and Engle (2017), consider individual capitalization with respect to that of the market. Similarly, Adrian and Brunnermeier (2016) measure the conditional effect of deviations from median value-at-risk on the system value-at-risk.

In this work, we focus on financial connectedness in the spirit of Diebold and Yilmaz (2014). Based on the relatively straightforward methodology of (generalized) variance decompositions in a vector moving average model, their work makes an important contribution to this field and establishes a link with the network literature. Nevertheless, the Diebold and Yilmaz (2014) modeling approach is affected by two main limitations. First, based on parametric estimation, it is not adequate for the large cross-sections typically pervaded by systemic events. Second, time-series dynamics measurement is based on rolling estimation which, as argued by Korobilis and Yilmaz (2018), are overwhelmingly affected by the choice of the window size. We propose a new model which overcomes both shortcomings.

The *adjusted intra-day log range* is defined by Parkinson (1980) as

$$X_{it} := \frac{(p_{it,\text{high}} - p_{it,\text{low}})^2}{4 \log 2} \tag{1}$$

where $p_{it,\text{high}}$ and $p_{it,\text{low}}$ are the maximum and minimum prices, respectively, of the i-th stock on day t. As stressed by Alizadeh et al. (2002), such a volatility proxy is "highly efficient and robust to microstructure noise", whereas in Brownlees and Gallo (2010) it is found to outperform more sophisticated alternatives. Our novel approach to the measurement of connectedness based on those log ranges is motivated by two stylized facts, here documented on a panel composed by 329 constituents of the Standard & Poor 500 observed between January 4, 2000 and August 31, 2015.

(a) *Strong commonality.* Figure 1 reports, as a function of time, the time-varying proportion of variance accounted for by the $k = 1, 3$ first dynamic factors (in the time-varying factor model to be described in Section 2). An overwhelming share of variance stems from a few common factors. As a result, only negligible information is lost by treating all the dynamics in the panel as factor-driven.

(b) *Time-varying interdependencies.* Figure 2 reports rolling estimates of the 329×329 sample covariance matrix of these log ranges computed at selected dates. The time-variation in the magnitude of covariances appears clear and shows an increase of interdependencies during crisis periods as 2008. Note that, since time-variation is also typical in covariances, not just variances, marginal transformations, as a rule, cannot stabilize joint distributions.

In order to accommodate for both of these empirical findings, we propose a time-varying extension of the General Dynamic Factor Model (henceforth GDFM) originally proposed by Forni et al. (2000). In its original form, the GDFM is dealing with large second-order stationary panels of time series loading common factors via time-invariant filters — as opposed to the more popular factor models of the *static type* (studied, among many others, by Stock and Watson (2002) and Bai and Ng (2002)), in which common factors are loaded via scalar loadings rather than filters. As argued in Hallin and Lippi (2013) and Forni et al. (2015, 2017), consistent estimation of the static factor model requires rather stringent assumptions on the dynamic properties of the data, while the GDFM follows from a very general representation result.

The essence of the GDFM is that few unobserved factors drive the main comovements across the panel where comovements are not only contemporaneous but can also be of dynamic nature, e.g. a factor may affect series i at time t but series j at time $t+1$. Such common factors, which in our context can be considered as "market wide" factors, generate the dynamic interdependencies across the observed log ranges which are the focus of this paper. The dynamic specification of the loadings in the GDFM is particularly useful in this context since filters naturally induce measures of connectedness at different time scales obtained from the impulse response functions of the observed data to the factors, and the implied variance decomposition.

Piecewise stationary factor models, in which parameters change in an abrupt way, also have been considered in order to cope with (a) and (b), with the desirable feature of spotting the exact location in time of structural breaks; that change-point approach in high dimension runs into hard problems, though — see e.g. Barigozzi et al. (2018) and references therein. Here, we rather adopt a time-varying extension of the GDFM, based on the locally stationary framework introduced by Dahlhaus (1997) and considered in Eichler et al. (2011), which assumes a second-order structure varying smoothly over time. Factor models with static time-varying loadings have been studied by Mikkelsen et al. (2018), Su and Wang (2017), Bates et al. (2013), Motta et al. (2011) and Del Negro and Otrok (2008).

However, the statistical treatment in Eichler et al. (2011), inspired by Forni et al. (2000), is based on dynamic principal component regression, which involves two-sided filters and therefore does not allow for any impulse response analysis of the dynamic effects of common factors on observed data. In the stationary context, an alternative estimation method therefore has been proposed by Forni et al. (2015, 2017), which is entirely based on one-sided filters. The estimation method we are proposing here is an extension to the time-varying GDFM of the same — equivalently, an alternative, involving one-sided filters only, to Eichler et al. (2011). By means of our time-varying GDFM, we therefore obtain time-dependent impulse responses and measures of connectedness.

Our approach to the study of connectedness at possibly different time scales is in the same spirit as a number of earlier works where components of financial data with different degrees of persistence are obtained for systemic risk analysis (Bandi and Tamoni, 2017) and closely related fields like asset pricing (Balke and Wohar, 2002; Ortu et al., 2013; Dew-Becker and Giglio, 2016), risk management (Engle, 2010), investment, employment and R&D (Barrero et al., 2017). Albeit applied to the low-dimensional framework of Diebold and Yilmaz (2014), a frequency domain decomposition of connectedness matrices similar to the one we perform here, is obtained by Baruník and Křehlík (2018).

Korobilis and Yilmaz (2018) also perform time-varying estimation of high-dimensional connectedness matrices; however, they do so using Bayesian shrinkage and stick to the vec-

tor autoregressive approach of Diebold and Yilmaz (2014) in which connectedness is directional between any two given variables. On the contrary, motivated by the fact that cross-dependencies in log range data are predominantly driven by common factors, the connectedness of each variable, in our approach, lies in its commonality and is undirectional. Indeed, in line with Acharya et al. (2017) and Adrian and Brunnermeier (2016), the connectedness measure associated with each variable in our GDFM model is its own contribution to the total connectedness of the whole system.

Also closely related to our work is Barigozzi and Hallin (2017) who, in a stationary high-dimensional GDFM consider connectedness generated by idiosyncratic factors. Although quantitatively unimportant in our data, idiosyncrasy may still be the object of interest and in the Appendix we show that zero-frequency coherence among idiosyncratic components display cross-sectional dependence with a block-wise pattern induced by the partition of data into industrial sectors.

Finally, sharing the opinion of Diebold and Yilmaz (2014), who urge for an increased integration of network theory techniques into multivariate econometric models for financial connectedness, we analyse the graph arising from our connectedness measures. So doing, we contribute to this strand of literature (see Billio et al., 2012; Allen et al., 2012; Acemoglu et al., 2010, to quote only a few) by proposing a time-varying network analysis.

When applying our approach to the S&P panel of log ranges, our main findings are the following:

(a) connectedness is much stronger (and relatively stable) at mid to low frequencies;

(b) large increases in long-run connectedness are associated with, and often anticipate, the main financial downturns;

(c) the largest spike in long-run connectedness associated with the great crisis of 2007–2009 is much amplified in banks, firms in related financial sectors and real estate;

(d) heterogeneity in long-run connectedness across sectors is relatively low in calm times and very high during financial turmoils.

The rest of the paper is organized as follows. In Section 2, we present the time-varying General Dynamic Factor Model. Building on Dahlhaus (2009), Eichler et al. (2011), and Forni et al. (2015, 2017), Section 3 proposes an estimation method, yielding consistent estimates of the time-varying impulse response functions to common shocks. Section 4 is about the connectedness measures we derive from the model and other techniques borrowed from network theory. Empirical results are discussed in Section 5. Section 6 concludes and outlines avenues for future research.

2 A time-varying Generalized Dynamic Factor Model

In this section we first define a time-varying Generalized Dynamic Factor Model (GDFM) inspired by Dahlhaus (1997, 2009) and Eichler et al. (2011). All random variables considered below belong to the space of centered real-valued random variables with finite second-order moments defined over some common probability space. As usual, L stands for the lag operator.

The factor model approach in the analysis of a (zero-mean) double-indexed process $\mathbf{X} := \{X_{it} : i \in \mathbb{N}_0,\ t \in \mathbb{Z}\}$ (here, the process of intraday log range values; i is

a cross-sectional index and t stands for time) is based on a decomposition of X_{it} into the sum

$$X_{it} = \chi_{it} + \xi_{it}, \quad i \in \mathbb{N}_0,\ t \in \mathbb{Z} \tag{2}$$

of two unobserved components: the common component process $\boldsymbol{\chi} := \{\chi_{it}\}$ and the idiosyncratic component process $\boldsymbol{\xi} := \{\xi_{it}\}$. For $\boldsymbol{\chi}$ and $\boldsymbol{\xi}$, we assume the following time-varying MA representations, which account for non-stationarity and the time-varying nature of their second-order structure:

$$\chi_{it} = \sum_{j=1}^{q} \sum_{k=0}^{\infty} c^*_{ijk}(t) u_{j,t-k}, \quad i \in \mathbb{N}_0,\ t \in \mathbb{Z}, \tag{3}$$

$$\xi_{it} = \sum_{j=1}^{\infty} \sum_{k=0}^{\infty} d^*_{ijk}(t) \eta_{j,t-k}, \quad i \in \mathbb{N}_0,\ t \in \mathbb{Z} \tag{4}$$

(see Assumption (A) for identification assumptions). Denoting by $\{\mathbf{X}_{nt} := (X_{1t}, \ldots, X_{nt})'\}$, $\{\boldsymbol{\chi}_{nt} := (\chi_{1t}, \ldots, \chi_{nt})'\}$, and $\{\boldsymbol{\xi}_{nt} := (\xi_{1t}, \ldots, \xi_{nt})'\}$ the n-dimensional subprocesses of $\mathbf{X}$, $\boldsymbol{\chi}$, and $\boldsymbol{\xi}$, we also have

$$\mathbf{X}_{nt} = \boldsymbol{\chi}_{nt} + \boldsymbol{\xi}_{nt}, \quad t \in \mathbb{Z},\ n \in \mathbb{N}_0$$

with

$$\boldsymbol{\chi}_{nt} := \mathbf{C}^*_n(t, L)\mathbf{u}_t \quad \text{and} \quad \boldsymbol{\xi}_{nt} := \mathbf{D}^*_n(t, L)\boldsymbol{\eta}_t, \quad t \in \mathbb{Z},\ n \in \mathbb{N}_0 \tag{5}$$

where $\mathbf{u}_t := (u_{1t}, \ldots, u_{qt})'$, $\boldsymbol{\eta}_t := (\eta_{1t}, \eta_{2t}, \ldots)'$,

$$\mathbf{C}^*_n(t, L) := \begin{pmatrix} c^*_{11}(t, L) & \ldots & c^*_{1q}(t, L) \\ \vdots & & \vdots \\ c^*_{n1}(t, L) & \ldots & c^*_{nq}(t, L) \end{pmatrix}, \quad \mathbf{D}^*_n(t, L) := \begin{pmatrix} d^*_{11}(t, L) & d^*_{12}(t, L) & \ldots \\ \vdots & \vdots & \\ d^*_{n1}(t, L) & d^*_{n2}(t, L) & \ldots \end{pmatrix},$$

$$c^*_{ij}(t, L) := \sum_{k=0}^{\infty} c^*_{ijk}(t) L^k, \quad 1 \le i \le n,\ 1 \le j \le q,$$

and

$$d^*_{ij}(t, L) := \sum_{k=0}^{\infty} d^*_{ijk}(t) L^k, \quad 1 \le i \le n,\ j \in \mathbb{N}_0.$$

The existence of time-independent one-sided filters $\mathbf{C}^*_n(t, L) = \mathbf{C}^*_n(L)$ is justified in the stationary case by the representation results in Hallin and Lippi (2013); here we directly assume (3). The generic element $c^*_{ij}(t, L)$ of $\mathbf{C}^*_n(t, L)$ represents the time-varying impulse response function of variable X_{it} to the jth factor (common shock) u_j; those impulse-response functions are the main quantities of interest here.

Throughout we assume that the shocks are satisfying the following assumption.

Assumption (A). *The common and idiosyncratic shocks are such that*

A1. the process of common shocks $\{\mathbf{u}_t : t \in \mathbb{Z}\}$ *is Gaussian second-order* q*-dimensional white noise:* $\mathrm{E}[\mathbf{u}_t] = \mathbf{0}$, $\mathrm{E}[\mathbf{u}_t \mathbf{u}_t'] = \mathbf{I}_q$, *and* $\mathrm{E}[\mathbf{u}_t \mathbf{u}_{t-k}]' = \mathbf{0}$ *for all* $t, k \in \mathbb{Z}$, *and* $k \neq 0$*;*

A2. the infinite-dimensional process of idiosyncratic shocks $\boldsymbol{\eta} := \{\boldsymbol{\eta}_t : t \in \mathbb{Z}\}$ *is Gaussian second-order white noise: for any* n*-dimensional subprocess* $\{\boldsymbol{\eta}_{nt} = (\eta_{1t}, \ldots, \eta_{nt})' : t \in \mathbb{Z}\}$, $\mathrm{E}[\boldsymbol{\eta}_{nt}] = \mathbf{0}$, $\mathrm{E}[\boldsymbol{\eta}_{nt} \boldsymbol{\eta}_{nt}'] = \mathbf{I}_n$, *and* $\mathrm{E}[\boldsymbol{\eta}_{nt} \boldsymbol{\eta}_{n,t-k}'] = \mathbf{0}$ *for all* $t, k \in \mathbb{Z}$, *and* $k \neq 0$*;*

A3. the common and idiosyncratic shocks are mutually orthogonal at all leads and lags: $\mathrm{E}[\eta_{i,t-k}u_{jt}] = 0$ *for all* $i \in \mathbb{N}_0$, $j = 1, \ldots, q$, *and* $t, k \in \mathbb{Z}$.

Gaussianity here is assumed for simplicity, as the adjusted intra-day log range observations we are considering in this paper are well approximated by Gaussian variables — see e.g. Alizadeh et al. (2002). Gaussian assumptions clearly could be relaxed — at the expense, however, of moment assumptions (as in Dahlhaus, 2009 or Eichler et al., 2011).

In practice, observations of $\mathbf{X}$ are available over a finite number T of points. Due to non-stationarity, letting T tend to infinity, that is, extending the process into the future, will not provide further insight into the behavior of the process at the beginning of the time interval. Hence, in this context, we need a different asymptotic scheme in order to assess the quality of inference procedures — typically, in order to study the consistency, as n and T tend to infinity, of estimators of the time-varying impulse response functions $\mathbf{C}_n^*(t, L)$ over the time interval $[1, T]$.

Following Dahlhaus (2009), we consider the *locally stationary* asymptotic scheme, an approach that has been initiated in Dahlhaus (1997). More precisely, for any $\tau \in [0, 1]$, let $\mathbf{X}_\tau = \{X_{it;\tau} : i \in \mathbb{N}_0,\ t \in \mathbb{Z}\}$ denote the fictitious (i.e., non-observable) stationary process described by the GDFM decomposition

$$X_{it;\tau} := \chi_{it;\tau} + \xi_{it;\tau}, \quad i \in \mathbb{N}_0,\ t \in \mathbb{Z}, \tag{6}$$

where

$$\chi_{it;\tau} = \sum_{j=1}^{q} \sum_{k=0}^{\infty} c_{ijk}(\tau) u_{j,t-k}, \quad i \in \mathbb{N}_0,\ t \in \mathbb{Z}, \tag{7}$$

$$\xi_{it;\tau} = \sum_{j=1}^{\infty} \sum_{k=0}^{\infty} d_{ijk}(\tau) \eta_{j,t-k}, \quad i \in \mathbb{N}_0,\ t \in \mathbb{Z}. \tag{8}$$

where the driving shocks u_{jt} and η_{jt} are the same as in (3) and (4) (hence satisfy Assumption (A)): write $\boldsymbol{\chi}_\tau$ and $\boldsymbol{\xi}_\tau$ for $\{\chi_{it:\tau} : i \in \mathbb{N}_0,\ t \in \mathbb{Z}\}$ and $\{\xi_{it:\tau} : i \in \mathbb{N}_0,\ t \in \mathbb{Z}\}$, respectively. Letting

$$\mathbf{X}_{nt;\tau} := (X_{1t;\tau}, \ldots, X_{nt;\tau})', \quad \boldsymbol{\chi}_{nt;\tau} := (\chi_{1t;\tau}, \ldots, \chi_{nt;\tau})', \text{ and } \boldsymbol{\xi}_{nt;\tau} := (\xi_{1t;\tau}, \ldots, \xi_{nt;\tau})',$$

(6)-(8) also can be written, with obvious notation $\mathbf{C}_n(\tau, L)$ and $\mathbf{D}_n(\tau, L)$, as

$$\mathbf{X}_{nt;\tau} = \boldsymbol{\chi}_{nt;\tau} + \boldsymbol{\xi}_{nt;\tau}, \quad \tau \in [0, 1],\ t \in \mathbb{Z},\ n \in \mathbb{N}_0 \tag{9}$$

where

$$\boldsymbol{\chi}_{nt;\tau} := \mathbf{C}_n(\tau, L)\mathbf{u}_t \quad \text{and} \quad \boldsymbol{\xi}_{nt;\tau} := \mathbf{D}_n(\tau, L)\boldsymbol{\eta}_{nt}, \quad \tau \in [0, 1],\ t \in \mathbb{Z},\ n \in \mathbb{N}_0. \tag{10}$$

As τ ranges over $[0, 1]$, the $\mathbf{X}_\tau$'s thus constitute a collection of stationary processes. Denote by $\mathbf{X}_T := \{X_{it} : i \in \mathbb{N}_0,\ t = 1, \ldots, T\}$ the finite-T subprocess of the nonstationary $\mathbf{X}$. The idea consists in approximating the (nonstationary) component X_{it} of $\mathbf{X}_T$ with the value $X_{it;t/T}$ of the stationary process $\mathbf{X}_\tau = \{X_{is;\tau} : i \in \mathbb{N}_0,\ s \in \mathbb{Z}\}$, $\tau = t/T$ (the so-called *rescaled time*) at time $s = t$:

$$X_{it} \approx X_{it;t/T} = \chi_{it;t/T} + \xi_{it;t/T}, \quad i \in \mathbb{N}_0,\ t = 1, \ldots, T, \tag{11}$$

where $\chi_{it;t/T}$, defined in (7), depends on the coefficients $c_{ijk}(t/T)$ and $\xi_{it;t/T}$, defined in (8), similarly depends on the coefficients $d_{ijk}(t/T)$.

If the approximation (11) is to make sense, of course, the coefficients in (7) and (8) need to satisfy some regularity assumptions, and to somehow approximate those in (3) and (4). The following regularity conditions are extending to the GDFM context Assumption 2.1 of Dahlhaus (2009) (see also Assumption 5 in Eichler et al., 2011, and note that Assumption (B4) is actually borrowed from Definition 2.1 in Dahlhaus, 1997).

ASSUMPTION (B). *There exist a $\kappa > 0$ and constants C_1, ..., C_4 (independent of i, j, and T) such that, letting*

$$\ell(k) := \begin{cases} 1 & \text{if } |k| \leq 1 \\ |k| \log^{1+\kappa} |k| & \text{if } |k| > 1 \,, \end{cases}$$

B1. $\sup_t |c^*_{ijk}(t)| \leq C_1/\ell(k)$ *for all* $i \in \mathbb{N}_0$, $j = 1, \ldots, q$, *and* $k \in \mathbb{N}$;

B2. $\sup_\tau |c_{ijk}(\tau)| \leq C_2/\ell(k)$ *for all* $i \in \mathbb{N}_0$, $j = 1, \ldots, q$, *and* $k \in \mathbb{N}$;

B3. $\sup_{m \in \mathbb{N}_0} \sup_{0=s_0 \leq \ldots \leq s_m = 1} \sum_{h=1}^m |c_{ijk}(s_h) - c_{ijk}(s_{h-1})| \leq C_3/\ell(k)$ *(that is, $\tau \mapsto c_{ijk}(\tau)$ has bounded variation) for all* $i \in \mathbb{N}_0$, $j = 1, \ldots, q$, *and* $k \in \mathbb{N}$;

B4. the coefficients $c^*_{ijk}(t)$ in (3) and $c_{ijk}(\tau)$ in (7) are related by

$$\max_{t=1,\ldots,T} \sup_{k \in \mathbb{N}} |c^*_{ijk}(t) - c_{ijk}(t/T)| \leq C_4/T$$

for all $i \in \mathbb{N}_0$, $j = 1, \ldots, q$, *and* $T \in \mathbb{N}_0$;

B5. analogs of conditions B1-B4 hold for the idiosyncratic coefficients $d^*_{ijk}(t)$ and $d_{ijk}(\tau)$ (with $j \in \mathbb{N}_0$ instead of $j = 1, \ldots, q$).

Although the filters in (7) and (8) are not required to coincide with those in (3) and (4), the approximation in (11) is justified by conditions B4 and B5. As we show in Section 3, this plays an essential role in the problem of consistent (as n and T tend to infinity) estimation of the impulse response coefficients $c^*_{ijk}(t)$. In accordance with Dahlhaus' terminology, a sequence of processes $\mathbf{X}_T$ satisfying Assumptions (A) and (B) will be called *locally stationary*.

Unlike the nonstationary $\mathbf{X}$, $\boldsymbol{\chi}$, and $\boldsymbol{\xi}$, the stationary processes $\mathbf{X}_\tau$, $\boldsymbol{\chi}_\tau$, and $\boldsymbol{\xi}_\tau$, for any $\tau \in [0, 1]$, under Assumptions (A) and (B), admit well-defined spectral densities. For any $n \in \mathbb{N}_0$, denote by

$$\boldsymbol{\Sigma}^X_n(\tau; \theta) := \frac{1}{2\pi} \sum_{k=-\infty}^{\infty} e^{-\iota k \theta} \, \mathrm{E}[\mathbf{X}_{nt;\tau} \mathbf{X}'_{n,t-k;\tau}], \qquad \theta \in (0, 2\pi], \tag{12}$$

the $n \times n$ spectral density matrix of $\mathbf{X}_{nt;\tau}$, and similarly define $\boldsymbol{\Sigma}^\chi_n(\tau; \theta)$ and $\boldsymbol{\Sigma}^\xi_n(\tau; \theta)$. For given τ and θ, each of the matrix sequences $\boldsymbol{\Sigma}^X_n(\tau; \theta)$, $\boldsymbol{\Sigma}^\chi_n(\tau; \theta)$, and $\boldsymbol{\Sigma}^\xi_n(\tau; \theta)$ is nested as n increases. Denote by $\lambda^X_{j;n}(\tau; \theta)$, $\lambda^\chi_{j;n}(\tau; \theta)$, and $\lambda^\xi_{j;n}(\tau; \theta)$ their jth eigenvalues (in decreasing order of magnitude). We make the following assumptions (see also Assumptions 2 and 3 in Eichler et al., 2011).

ASSUMPTION (C). *C1. For any $n \in \mathbb{N}_0$ and $\theta \in (0, 2\pi]$, the mappings $\tau \mapsto \boldsymbol{\Sigma}^\chi_n(\tau; \theta)$ and $\tau \mapsto \boldsymbol{\Sigma}^\xi_n(\tau; \theta)$ are Lipschitz continuous;*

C2. the spectral density matrices $\mathbf{\Sigma}_n^{\chi}(\tau;\theta)$ *and* $\mathbf{\Sigma}_n^{\xi}(\tau;\theta)$ *are twice continuously differentiable for all* $\tau \in [0,1]$ *and all* $\theta \in (0,2\pi]$*;*

C3. there exist continuous functions $\theta \mapsto \alpha_j^{\chi}(\tau;\theta)$ *and* $\theta \mapsto \beta_j^{\chi}(\tau;\theta)$ *,* $j = 1,\dots,q$*, and an integer* N_χ *such that, for all* $n > N_\chi$*, all* $\tau \in [0,1]$*, and Lebesgue-a.e.*[1] *over* $\theta \in (0,2\pi]$*,*

$$\beta_1^{\chi}(\tau;\theta) \geq \frac{\lambda_{1;n}^{\chi}(\tau;\theta)}{n} \geq \alpha_1^{\chi}(\tau;\theta) > \beta_2^{\chi}(\tau;\theta) \geq \frac{\lambda_{2;n}^{\chi}(\tau;\theta)}{n} \geq \dots$$
$$\dots \geq \alpha_{q-1}^{\chi}(\tau;\theta) > \beta_q^{\chi}(\tau;\theta) \geq \frac{\lambda_{q;n}^{\chi}(\tau;\theta)}{n} \geq \alpha_q^{\chi}(\tau;\theta) > 0;$$

C4. there exists a constant B_ξ *such that* $\lambda_{1;n}^{\xi}(\tau;\theta) \leq B_\xi$ *for all* $n \in \mathbb{N}_0$*, all* $\tau \in [0,1]$ *and all* $\theta \in (0,2\pi]$*.*[2]

Assumption (C) is a generalization to the time-varying case of the classical assumption of an eigen-gap in the spectral density matrix which is increasing with n and therefore allows for identification of the common and idiosyncratic components as $n \to \infty$ (Forni et al., 2000). Note that C3 rules out the possibility of a time-varying number of factors: irrespective of τ, all spectral density matrices $\mathbf{\Sigma}_n^{\chi}(\tau;\theta)$ have (for $n \geq q+1$) q distinct and exploding (as $n \to \infty$) eigenvalues.

Assuming that the nT-dimensional process $\mathbf{X}_{nT} := \{X_{it} : \ i = 1,\dots,n, \ t = 1,\dots,T\}$ (an $n \times T$ panel) is observed, associate with each $t = 1,\dots,T$ the spectral density matrices $\mathbf{\Sigma}_n^{X}(t/T;\theta)$, $\mathbf{\Sigma}_n^{\chi}(t/T;\theta)$, and $\mathbf{\Sigma}_n^{\xi}(t/T;\theta)$: those spectral matrices, which depend on rescaled time, will be used as local substitutes for $\mathbf{X}_{nT}$'s nonexisting (or meaningless) spectrum. Obviously,

$$\mathbf{\Sigma}_n^{X}(t/T;\theta) = \mathbf{\Sigma}_n^{\chi}(t/T;\theta) + \mathbf{\Sigma}_n^{\xi}(t/T;\theta), \quad t = 1,\dots,T, \ \theta \in (0,2\pi].$$

We conclude this section with assuming the existence of a singular autoregressive representation for the common components processes $\boldsymbol{\chi}_\tau$ (for a stationary version, see Assumption 5 in Forni et al., 2017).

Assumption (D). *Denote by* $\boldsymbol{\chi}_\tau^{(q+1)} := \{\boldsymbol{\chi}_{t;\tau}^{(q+1)} := (\chi_{i_1 t;\tau},\dots,\chi_{i_{q+1} t;\tau})' : t \in \mathbb{Z}\}$ *an arbitrary* $(q+1)$*-dimensional subprocess of* $\boldsymbol{\chi}_\tau$ *(as defined in* (7)*). For all* $\tau \in [0,1]$ *and* $k \in \mathbb{N}_0$*,*

D1. there exists a unique autoregressive $(q+1)\times(q+1)$ *filter* $\mathbf{A}^{(q+1)}(\tau,L)$ *and a* $(q+1)\times q$ *matrix* $\mathbf{H}^{(q+1)}(\tau)$ *of rank* q *such that*

$$\mathbf{A}^{(q+1)}(\tau,L)\boldsymbol{\chi}_{t;\tau}^{(q+1)} = \mathbf{H}^{(q+1)}(\tau)\mathbf{u}_t, \quad t \in \mathbb{Z};$$

D2. the order of $\mathbf{A}^{(q+1)}(\tau,L)$ *is bounded, uniformly in* $\tau \in [0,1]$ *and* $(i_1,\dots,i_{q+1})$*, by some* $S \geq 0$*;*

D3. $\det \mathbf{A}^{(q+1)}(\tau,z) \neq 0$*, for all* $z \in \mathbb{C}$ *such that* $|z| \leq 1$*;*

[1] that is, except for a subset of θ values included in a set with Lebesgue measure zero.

[2] Assumption 4 in Forni et al. (2017) provides (mutatis mutandis) sufficient conditions for this, involving the coefficients $d_{ijk}(\tau)$.

D4. let $\mathbf{\Gamma}^{\chi^{(q+1)}}(\tau,\ell) = \mathrm{E}[\boldsymbol{\chi}_{t;\tau}^{(q+1)}\boldsymbol{\chi}_{t-k;\tau}^{(q+1)\prime}]$ *denote the* $(q+1)\times(q+1)$ *lag* ℓ *autocovariance matrix of* $\boldsymbol{\chi}_{\tau}^{(q+1)}$ *and, for* $S>0$*, define the* $S(q+1)\times S(q+1)$ *matrix*

$$\mathbf{G}^{(q+1)}(\tau) := \begin{pmatrix} \mathbf{\Gamma}^{\chi^{(q+1)}}(\tau,0) & \mathbf{\Gamma}^{\chi^{(q+1)}}(\tau,1) & \dots & \mathbf{\Gamma}^{\chi^{(q+1)}}(\tau,S-1) \\ \mathbf{\Gamma}^{\chi^{(q+1)}}(\tau,-1) & \mathbf{\Gamma}^{\chi^{(q+1)}}(\tau,0) & \dots & \mathbf{\Gamma}^{\chi^{(q+1)}}(\tau,S-2) \\ \vdots & \vdots & \ddots & \vdots \\ \mathbf{\Gamma}^{\chi^{(q+1)}}(\tau,-S+1) & \mathbf{\Gamma}^{\chi^{(q+1)}}(\tau,-S+2) & \dots & \mathbf{\Gamma}^{\chi^{(q+1)}}(\tau,0) \end{pmatrix}:$$

there exists a constant $d>0$ *such that* $\det \mathbf{G}^{(q+1)}(\tau) > d$*, for all* $(i_1,\dots,i_{q+1})$ *and all* $\tau\in[0,1]$*. For* $S=0$*, let* $\mathbf{G}^{(q+1)}(\tau) := \mathbf{I}_{q+1}$ *for all* $\tau\in[0,1]$*.*

Assumption (D) is crucial for allowing us to estimate the model by means of one-sided filters. Actually, it has been shown by Anderson and Deistler (2008a,b) that, for *rational processes*[3] it holds *generically*[4]. Generically is not enough here, though, and this is why we need to make it an assumption which, however, for the same reason, turns out to be a very mild one (see also Section 4 in Forni et al., 2015).

Now consider the case in which $n = m(q+1)$ for some integer m.[5] The n-dimensional common component $\boldsymbol{\chi}_{nt;\tau}$ under Assumption (D) admits the autoregressive representation

$$\mathbf{A}_n(\tau,L)\boldsymbol{\chi}_{nt;\tau} = \mathbf{R}_n(\tau)\mathbf{u}_t, \qquad \tau\in[0,1],\ t\in\mathbb{Z} \tag{13}$$

where, for all $\tau\in[0,1]$, $\mathbf{A}_n(\tau,L)$ is block-diagonal with m diagonal blocks $\mathbf{A}^k(\tau,L)$, $k=1,\dots,m$, each of dimension $(q+1)\times(q+1)$ and satisfying Assumption (D), and $\mathbf{R}_n(\tau)$ (stacking m matrices of the type $\mathbf{H}^{(q+1)}(\tau)$) is of dimension $n\times q$ with full column rank q. Moreover, letting $\mathbf{Z}_{nt;\tau} := \mathbf{A}_n(\tau,L)\mathbf{X}_{nt;\tau}$ we have

$$\mathbf{Z}_{nt;\tau} = \mathbf{R}_n(\tau)\mathbf{u}_t + \mathbf{A}_n(\tau,L)\boldsymbol{\xi}_{nt;\tau} =: \boldsymbol{\psi}_{nt;\tau} + \boldsymbol{\zeta}_{nt;\tau}, \qquad \tau\in[0,1],\ t\in\mathbb{Z}. \tag{14}$$

This defines for $\mathbf{Z}_{nt;\tau}$ a locally stationary *static* factor model with the same q common shocks $\{\mathbf{u}_t\}$ as those appearing in the definition (3) of the nonstationary GDFM for $\mathbf{X}$. Let $\mathbf{\Gamma}_n^Z(\tau)$, $\mathbf{\Gamma}_n^\psi(\tau)$, and $\mathbf{\Gamma}_n^\zeta(\tau)$ stand for the $n\times n$ covariance matrices of $\mathbf{Z}_{nt;\tau}$, $\boldsymbol{\psi}_{nt;\tau}$, and $\boldsymbol{\zeta}_{nt;\tau}$, respectively; because of Assumption (A3), we have

$$\mathbf{\Gamma}_n^Z(\tau) = \mathbf{\Gamma}_n^\psi(\tau) + \mathbf{\Gamma}_n^\zeta(\tau).$$

Let $\mu_{j;n}^\psi(\tau)$ and $\mu_{j;n}^\zeta(\tau)$ denote the jth eigenvalues (in decreasing order) of the covariance matrices $\mathbf{\Gamma}_n^\psi(\tau)$ and $\mathbf{\Gamma}_n^\zeta(\tau)$, respectively. Our last assumption allows us to identify the decomposition (14) as $n\to\infty$ (see Assumption 6 in Forni et al., 2017).

Assumption (E). *E1. There exist constants* $\alpha_j^\psi(\tau)$ *and* $\beta_j^\psi(\tau)$ *,* $j=1,\dots,q$*, and an integer* N_ψ *such that, for all* $n>N_\psi$*, and all* $\tau\in[0,1]$*,*

$$\beta_1^\psi(\tau) \geq \frac{\mu_{1;n}^\psi(\tau)}{n} \geq \alpha_1^\psi(\tau) > \beta_2^\psi(\tau) \geq \frac{\mu_{2;n}^\psi(\tau)}{n} \geq \dots$$
$$\dots \geq \alpha_{q-1}^\psi(\tau) > \beta_q^\psi(\tau) \geq \frac{\mu_{q;n}^\psi(\tau)}{n} \geq \alpha_q^\psi(\tau) > 0;$$

[3] A rational process is a process admitting a VARMA representation of finite (but unspecified) orders; such processes are dense in the family of stationary processes.

[4] that is, except for a subset of the parameter space of their VARMA representation contained in a set of Lebesgue measure zero.

[5] This is convenient and does not imply any loss of generality for our asymptotic analysis, see the end Section 3.1 for further details when this is not the case.

E2. there exists a constant B_ζ such that $\mu^{\zeta}_{1;n}(\tau) \leq B_\zeta$ for all $n \in \mathbb{N}_0$ and all $\tau \in [0,1]$.

3 Estimation and consistency

In this section, we show how to adapt the Forni et al. (2015, 2017) one-sided estimation method to the time-varying setting described by Assumptions (A)-(E). The substantial advantage over the Eichler et al. (2011) time-varying extension of the simpler dynamic principal component analysis of Forni et al. (2000) is that it delivers estimators of the filters $\mathbf{C}^*_n(t,L)$ $(1 \leq t \leq T)$ which are one-sided and therefore can be directly used for time-varying impulse response analysis.

Hereafter, all estimated quantities are denoted with "hats", e.g. $\widehat{c}_{ij;n,T}(t/T)$ for the estimator, based on the observation of an $n \times T$ realization $\mathbf{X}_{nT}$ of $\mathbf{X}$, of the kth coefficient in the (i,j)th entry of $\mathbf{C}_n(t/T,L)$, etc. All estimated quantities depend on both n and T.

3.1 Estimation

Our estimation procedure is based on three main steps; throughout this section, n and T are fixed.

(i) Dynamic Principal Component Analysis. First, let J be a kernel with bandwidth b_T and K a kernel with bandwidth h_T, then, following Neumann and von Sachs (1997), we estimate the local spectral density matrices $\mathbf{\Sigma}^X_n(\tau;\theta)$ by means of the *smoothed pre-periodograms*

$$\widehat{\mathbf{\Sigma}}^X_{n,T}(\tau;\theta_j) := \frac{2\pi}{T^2 b_T h_T} \sum_{s=1}^{T}\sum_{\ell=1}^{T} \mathrm{J}\left(\frac{\tau T - s}{T b_T}\right) \mathrm{K}\left(\frac{\theta_j - \frac{2\pi\ell}{T}}{h_T}\right) \mathbf{S}_{n,T}(\tau;\theta_j),\ \tau \in [0,1], \quad (15)$$

which is the smoothed version of the *pre-periodograms*

$$\mathbf{S}_{n,T}(\tau;\theta_j) := \frac{1}{2\pi} \sum_{k:1 \leq \lfloor \tau T + \frac{1\pm k}{2} \rfloor \leq T} e^{-\iota k \theta_j} \mathbf{X}_{n,\lfloor \tau T + \frac{1+k}{2} \rfloor} \mathbf{X}'_{n,\lfloor \tau T + \frac{1-k}{2} \rfloor},\ \tau \in [0,1]. \quad (16)$$

and where (15) and (16) are computed on the set $\{\theta_j = 2\pi h_T j,\ j = 1,\ldots,\lfloor 1/h_T \rfloor\}$ of Fourier frequencies. Moreover, although τ ranges over $[0,1]$, both quantities in (15) and (16) for given θ_j only take a finite number T of distinct values, corresponding to a discrete set $\{1/T,\ldots,(T-1)/T,1\}$ of τ values. We refer to Section 5.1 for the specific choice of kernels and bandwidths. Here we just notice that the time bandwidth b_T is defined in rescaled time such that $\lfloor b_T T \rfloor$ corresponds to a given number of observations in the interval $[1,T]$ used to compute (15) at a given τ, while the frequency bandwidth h_T is defined over $(0,2\pi]$ such that $\lfloor h_T T/(2\pi) \rfloor$ is the number of frequencies used to compute (15) at a given θ. The estimator (15) as usual can be extended to arbitrary frequencies $\theta \in (0,2\pi]$ as[6]

$$\widehat{\mathbf{\Sigma}}^X_{n,T}(\tau;\theta) := \widehat{\mathbf{\Sigma}}^X_{n,T}(\tau;\theta_j) \quad \text{for } \theta_{j-1} < \theta \leq \theta_j,$$

[6]However, note that, while in principle we could compute (15) over a finer grid, e.g. $\theta_j = 2\pi j/T$ with $j = 1,\ldots,T$, in practice, due to the smoothing, the maximum achievable resolution is $1/(2\pi h_T) < T/2\pi$, because of Assumption (F) below.

with $\theta_0 := 0$.

For any given T, n, τ, and θ, denote by $\widehat{\lambda}^X_{j;n,T}(\tau;\theta)$ the jth eigenvalue (in decreasing order of magnitude) of $\widehat{\mathbf{\Sigma}}^X_{n,T}(\tau;\theta)$ and by $\widehat{\mathbf{P}}^X_{j;n,T}(\tau;\theta)$, the corresponding n-dimensional normalized eigenvector. Then, for a given number q of factors,

$$\widehat{\mathbf{\Sigma}}^\chi_{n,T}(\tau;\theta) := \sum_{j=1}^{q} \widehat{\lambda}^X_{j;n,T}(\tau;\theta)\widehat{\mathbf{P}}^X_{j;n,T}(\tau;\theta)\widehat{\mathbf{P}}^{X\dagger}_{j;n,T}(\tau;\theta),\ \tau\in[0,1]$$

is an estimator of the spectral density $\mathbf{\Sigma}^\chi_n(\tau;\theta)$ of the common component at frequency θ.

Lastly, by inverse Fourier transform, we compute, for $\tau = t/T$, estimators of the local autocovariance matrices of the common component:

$$\widehat{\mathbf{\Gamma}}^\chi_{n,T}(t/T,k) := 2\pi\lfloor h_T\rfloor \sum_{j=1}^{\lfloor 1/h_T\rfloor} e^{\iota k\theta_j}\ \widehat{\mathbf{\Sigma}}^\chi_{n,T}(t/T;\theta_j),\quad t=1,\dots,T,\ k\in\mathbb{Z}. \tag{17}$$

(ii) VAR filtering. Assuming again, for simplicity, that $n = m(q+1)$ for some integer m, write $\boldsymbol{\chi}^k_{nt;\tau} := (\chi_{(k-1)(q-1)+1,t;\tau},\dots,\chi_{k(q+1),t;\tau})'$, $k=1,\dots,m$, for the m $(q+1)$-dimensional subvectors of $\boldsymbol{\chi}_{nt;\tau}$, and consider the m autoregressive models each of dimension $(q+1)$ (see Assumption (D))

$$\mathbf{A}^k_n(t/T,L)\boldsymbol{\chi}^k_{nt;t/T} = \mathbf{H}^k_n(t/T)\mathbf{u}_t,\quad t=1,\dots,T,\ k=1,\dots,m. \tag{18}$$

Based on the estimated autocovariances (17), compute, using AIC for the VAR orders, the Yule-Walker estimates $\widehat{\mathbf{A}}^k_{n,T}(t/T,L)$ of the autoregressive filters $\mathbf{A}^k_n(t/T,L)$. Construct the $n\times n$ block-diagonal filter $\widehat{\mathbf{A}}_{n,T}(t/T,L)$ with (see (13)) the m diagonal blocks $\widehat{\mathbf{A}}^1_{n,T}(t/T,L),\dots,\widehat{\mathbf{A}}^m_{n,T}(t/T,L)$ and the filtered process

$$\widehat{\mathbf{Z}}_{nt;t/T} := \widehat{\mathbf{A}}_{n,T}(t/T,L)\mathbf{X}_{nt},\quad t=1,\dots,T \tag{19}$$

which will be used as an estimation of $\mathbf{Z}_{nt;t/T}$, where $\mathbf{Z}_{nt;t/T}$ satisfies (for $\tau = t/T$) (14).

(iii) Principal Component Analysis. Following Rodríguez-Poo and Linton (2001), we consider the smoothed covariance matrix

$$\widehat{\mathbf{\Gamma}}^{\hat{Z}}_{n,T}(t/T) := \frac{1}{T}\sum_{s=1}^{T} \mathrm{J}\left(\frac{t-s}{Tb_T}\right)\widehat{\mathbf{Z}}_{ns;t/T}\widehat{\mathbf{Z}}'_{ns;t/T},\quad t=1,\dots,T, \tag{20}$$

of $\widehat{\mathbf{Z}}_{nt;t/T}$, where the kernel J is the same as the one used in (15) for computing the local spectral density. Denote by $\widehat{\mu}^{\hat{Z}}_{j;n,T}(t/T)$ the jth eigenvalue of $\widehat{\mathbf{\Gamma}}^{\hat{Z}}_n(t/T)$ in decreasing order of magnitude, with normalized n-dimensional eigenvector $\widehat{\mathbf{P}}^{\hat{Z}}_{j;n,T}(t/T)$; define

$$\widehat{\mathbf{R}}_{j;n,T}(t/T) := \widehat{\mathbf{P}}^{\hat{Z}}_{j;n,T}(t/T)\sqrt{\widehat{\mu}^{\hat{Z}}_{j;n,T}(t/T)},\quad j=1,\dots,q,$$

and let $\widehat{\mathbf{R}}_{n,T}(t/T) := (\widehat{\mathbf{R}}_{1;n,T}(t/T)\dots\widehat{\mathbf{R}}_{q;n,T}(t/T))$. Our estimators of the impulse response functions $\mathbf{C}^*_n(t,L)$ are

$$\widehat{\mathbf{C}}^*_{n,T}(t,L) := [\widehat{\mathbf{A}}_{n,T}(t/T,L)]^{-1}\widehat{\mathbf{R}}_{n,T}(t/T). \tag{21}$$

with (i,j) entry $\widehat{\mathbf{c}}^*_{ij;n,T}(t,L) =: \sum_{k=0}^{\infty}\widehat{\mathbf{c}}^*_{ijk;n,T}(t)L^k$; the latter, up to a q-tuple of signs (see Proposition 1), is a consistent estimator of $\mathbf{c}^*_{ij}(t,L) =: \sum_{k=0}^{\infty}\mathbf{c}^*_{ijk}(t)L^k$ as $n,T\to\infty$.

The estimation procedure just described calls for some comments. First, step *(i)* is directly taken from Eichler et al. (2011), who propose to estimate the common component by means of time-varying dynamic principal components. Steps *(ii)* and *(iii)*, and the estimator (21) of the time-varying impulse response function to common shocks represent the novelty of this paper, being the generalization to the time-varying case of the approach proposed by Forni et al. (2017). In particular, step *(iii)* shows how an adequate VAR filtering brings the problem back to a time-varying static factor model in the style of Rodríguez-Poo and Linton (2001) and Motta et al. (2011).

Second, the matrices $\mathbf{R}_n(\tau)$ and the noise $\mathbf{u}_t$ in (13) are identified up to an arbitrary orthogonal transformation $\mathbf{P}_t$ only, as $\mathbf{R}_n(\tau)\mathbf{u}_t = \mathbf{R}_n(\tau)\mathbf{P}_t\mathbf{P}_t'\mathbf{u}_t$. It is shown in the Appendix that our choice of $\widehat{\mathbf{R}}_{n,T}(t/T)$ identifies the impulse responses up to a sign. This, however, is not surprising, as the shocks have been assumed to be Gaussian, hence suffer the same indetermination. That sign issue can be solved by imposing identification constraints: see, for instance, Section 4.1 in Forni et al. (2009). Since, however, our study of connectedness does not require specifying those signs, we are skipping details.

Third, the cross-sectional ordering of the panel has an impact on the selection of the m subvectors $\boldsymbol{\chi}^k_{nt;\tau}$ in step *(ii)* and the possible dropping of $n - \lfloor n/(q+1) \rfloor (q+1)$ series at the end of the panel when n is not an exact multiple of $(q+1)$. The $n!$ cross-sectional permutations of the panel, thus, would lead to $n!$ estimators, all sharing the same consistency properties stated in Proposition 1. A Rao-Blackwell argument (see Section 3.5 of Forni et al., 2017 for details) suggests aggregating these estimators into a unique one by simple averaging (after obvious reordering) of the resulting impulse response functions. Although averaging over all $n!$ permutations is clearly unfeasible, as stressed by Forni et al. (2017, Section 4.2) and Forni et al. (2018, Appendix D) in a stationary setting, a few of them are enough, in practice, to deliver stable averages (which therefore are matching the infeasible average over all $n!$ permutations). Such averaging clearly has no impact on consistency.

Fourth, the number q of common shocks throughout has been considered as known, and we assumed it to be constant through time. That number has to be estimated from the observations, though. We suggest using the criterion proposed by Hallin and Liška (2007). However, instead of implementing it on the basis of a classical periodogram (invalid in the present context), we suggest running the method on the the smoothed pre-periodogram $\widehat{\boldsymbol{\Sigma}}^X_{n,T}(1/2;\theta)$ associated with the middle part of the observation period ($\tau = 1/2$). The validity of the assumption of a constant number q of common shocks also can be tested heuristically by iterating the same analysis for a few values of τ, then comparing the results[7].

3.2 Consistency

We now turn to the consistency, as n and T tend to infinity, of the estimated time-varying impulse response functions (21). This, however, requires assumptions on the bandwidths and the kernels used in (15).

Assumption (F). *The kernels* J *and* K

F1. have compact support $[-1/2, 1/2]$*;*

F2. are such that $\int_{-1/2}^{1/2} x\mathrm{J}(x)\mathrm{d}x = \int_{-1/2}^{1/2} x\mathrm{K}(x)\mathrm{d}x = 0$ *and* $\int_{-1/2}^{1/2} \mathrm{J}(x)\mathrm{d}x = \int_{-1/2}^{1/2} \mathrm{K}(x)\mathrm{d}x = 1$.

[7] This is how we determine q in Section 5.

The bandwidths h_T and b_T are such that, as $T \to \infty$,

F3. $h_T \to 0$, $b_T \to 0$, $Th_Tb_T \to \infty$, $Th_Tb_T/\log^2 T \to \infty$, *and* $\sqrt{Th_Tb_T}(h_T^2 + b_T^2) \to 0$.

Let $\widehat{\sigma}^X_{ij;n,T}(\tau;\theta)$ and $\sigma^X_{ij}(\tau;\theta)$ denote the (i,j) entries of $\widehat{\mathbf{\Sigma}}^X_{n,T}(\tau;\theta)$ and $\mathbf{\Sigma}^X_n(\tau,\theta)$, respectively (due to nestedness, $\sigma^X_{ij}(\tau;\theta)$ does not depend on n). It follows from Dahlhaus (2009, Example 4.2) (see also Theorem 7 in Eichler et al., 2011) that, under Assumptions (A), (B), and (F), as n and T tend to infinity,

$$\sup_{\tau\in\left[\frac{b_T}{2},1-\frac{b_T}{2}\right]}\sup_{\theta\in(0,2\pi]}\max_{i,j=1,\dots,n}\mathrm{E}\left[\left|\widehat{\sigma}^X_{ij;n,T}(\tau;\theta)-\sigma^X_{ij}(\tau;\theta)\right|^2\right]=O\left(\frac{1}{Th_Tb_T}\right). \tag{22}$$

Due to the two-sided kernel used for smoothing in time, the above result only holds for the central part of the observation period, not for the beginning nor the end of it. In particular, letting for example $t=\lfloor \tau T\rfloor$[8], (22) only holds for $t=\lfloor\frac{Tb_T}{2}\rfloor,\lfloor\frac{Tb_T}{2}\rfloor+1,\dots,T-\lfloor\frac{Tb_T}{2}\rfloor$, that is, for the central $T-\lfloor Tb_T\rfloor+1$ or $T-\lfloor Tb_T\rfloor+2$ values of t, according as $\lfloor Tb_T\rfloor$ is even or odd. A consequence is that, in Proposition 1 below (and assuming that Assumptions (C), (D), and (E) also hold), we only do recover the impulse response functions for the same central values of t.

Finally, consistency in the following proposition is considered in terms of the estimation of the coefficients $c^*_{ijk}(t)$. This, however, brings back the identification issue mentioned is Section 3.1. While that issue can be fixed by means of identification constraints, we do not need to resolve it here and, for the sake of simplicity, we keep the sign indetermination in the following consistency statement (a similar choice is made, for instance, in Propositions 10 and 11 of Forni et al., 2017).

Proposition 1. *Let Assumptions (A)-(F). For any given $k\geq 0$, there exist sequences $\{s_j(t)\}_{j=1}^q$, with $s_j(t)=\pm 1$, such that, as $n,T\to\infty$ with $n=O(T^\omega)$ for some $\omega>0$,*

$$\max_{t=\left\lfloor\frac{Tb_T}{2}\right\rfloor,\dots,T-\left\lfloor\frac{Tb_T}{2}\right\rfloor}\max_{\substack{i=1,\dots,n\\ j=1,\dots,q}}\left|\widehat{c}^*_{ijk;n,T}(t)-s_j(t)c^*_{ijk}(t)\right|=O_{\mathrm{P}}\left(\max\left(\sqrt{\frac{\log T}{Th_Tb_T}},\sqrt{\frac{\log T}{n}}\right)\right).$$

This consistency result is proved in the Appendix and it justifies, for large n and T, the analysis of connectedness to be conducted in the next section on the basis of $\widehat{\mathbf{C}}^*_{n,T}(t,z)$.

4 An analysis of (time-varying) connectedness

Turning to financial connectedness, our connectedness measurements, in analogy with Diebold and Yilmaz (2014), are based on the (empirical) $n\times n$ *connectedness matrices*

$$\mathbf{Q}_{n,T}(t,z):=\widehat{\mathbf{C}}^*_{n,T}(t,z)\widehat{\mathbf{C}}^{*\prime}_{n,T}(t,z),\qquad z\in\mathbb{C} \tag{23}$$

with $\widehat{\mathbf{C}}^*_{n,T}(t,z)$ defined in (21). Note that since $\widehat{\mathbf{C}}^*_{n,T}(t,z)$ represents the dynamic effect of the common "market-wide" shocks, considering (23) at different horizons yields connectedness measurements at different horizons: namely,

[8]This is the way we compute our estimators in Section 4, however notice that the choice $t=\lceil\tau T\rceil$ is equally valid.

(a) *a long-run connectedness matrix* at time t measured as $\mathbf{Q}_{n,T}(t,1)$ which is generated by the long-run effects of the market shocks;

(b) *an instantaneous connectedness matrix* at time t measured as $\mathbf{Q}_{n,T}(t,0)$ which is generated by the instantaneous effects the market shocks;

(c) *spectral connectedness matrices within specific frequency bands* $\Theta \subset (0, 2\pi]$ defined as the connectedness in the components with period $\frac{2\pi}{\theta}$ $(\theta \in \Theta)$ of the spectral representation[9] of $\mathbf{X}_{nt}$:

$$\mathbf{Q}_{n,T;\Theta}(t) \coloneqq \frac{1}{|\Theta|}\int_{\Theta} \mathbf{Q}_{n,T}\left(t, e^{-ik\theta}\right) d\theta, \tag{24}$$

where $|\Theta|$ stands for the size of the frequency band Θ.

Note that, due to its quadratic nature, $\mathbf{Q}_{n,T}(t,z)$ is not impacted by the sign issue in the definition of $\widehat{\mathbf{C}}^*_{n,T}(t,z)$. Throughout this section, n and T are fixed, and we simplify the notation by dropping the subscripts n, T, thus writing $\widehat{\mathbf{C}}^*_k(t)$, $\mathbf{Q}(t,z)$, etc.

The evolution in time of the norms of connectedness matrices provides an insight into the evolution of the total amount of connectedness generated, across the observed panel, by the common factors or shocks. It is also possible to obtain decompositions of that total amount into a sum of mutually orthogonal contributions attributable to each of the q common factors. Denoting by $\widehat{\mathbf{C}}^*_k(t)$ the kth matrix coefficient of the polynomial $\widehat{\mathbf{C}}^*(t,z)$ and by $\widehat{\mathbf{C}}^*_{\bullet jk}(t)$ the jth column of $\widehat{\mathbf{C}}^*_k(t)$, we have $\widehat{\mathbf{C}}^*_{\bullet j}(t,z) = \sum_{k=0}^{\infty} \widehat{\mathbf{C}}^*_{\bullet jk}(t) z^k$, a sum which in practice we truncate at $k_{\max} = 20$:

$$\widehat{\mathbf{C}}^*_{\bullet j}(t,z) = \sum_{k=0}^{k_{\max}} \widehat{\mathbf{C}}^*_{\bullet jk}(t) z^k$$

thus is the component of the filter $\widehat{\mathbf{C}}^*_n(t,z)$ corresponding to the impulse responses to the jth factor at time t, while

$$\mathbf{Q}_{\bullet j;n}(t,z) \coloneqq \widehat{\mathbf{C}}^*_{\bullet j;n}(t,z)\, \widehat{\mathbf{C}}^{*\prime}_{\bullet j;n}(t,z) \tag{25}$$

represents the contribution (at time t) of factor j to total connectedness; individual factor contributions to long-run, instantaneous, and spectral connectedness at time t are obtained similarly.

Cross-sectional decompositions also are possible: the connectedness of a specific cross-sectional item i attributable to factor j, and its *total connectedness* at time t can be measured as

$$Q_{ij}(t,z) \coloneqq \{\widehat{c}^*_{ij}(t,z)\}^2 \quad \text{and} \quad Q_{i\bullet}(t,z) \coloneqq \sum_{j=1}^{q} Q_{ij}(t,z), \tag{26}$$

respectively; definitions of long-run, instantaneous, and spectral connectedness of series i, due to factor j and total, follow in an obvious way. It will be convenient also to introduce i's *mean connectedness*[10] *at time* t $Q_i(t,z) \coloneqq \frac{1}{q} Q_{i\bullet}(t,z)$.

Finally, it is often useful to evaluate connectedness within a group of variables. Let $\mathcal{S}(k)$, with cardinality n_k, denote the set of indexes of the series belonging to some sector k. We can measure the corresponding sector-specific mean connectedness at time t as

$$\mathbf{Q}_{[\mathcal{S}(k),\bullet]}(t,z) \coloneqq \frac{1}{n_k} \sum_{i \in \mathcal{S}(k)} Q_i(t,z), \tag{27}$$

[9] See Theorem 11.8.2 in Brockwell and Davis (1991).

[10] Mean connectedness actually is what Diebold and Yilmaz (2014) call total connectedness.

from which we can compute the $n_k \times q$ matrices of sector-specific long-run, instantaneous, and spectral connectedness. With obvious notation, $\mathbf{Q}_{[\mathcal{S}(k),j]}(t,z)$ is the n_k-dimensional component of $\mathbf{Q}_{[\mathcal{S}(k),\bullet]}(t,z)$ related to the jth factor at time t.

4.1 Network interpretation of connectedness measures

As illustrated by Diebold and Yilmaz (2014), covariances are closely related to network analysis. We share their view that the "blend of multivariate time series and network literature has much to contribute to the successful measurement of financial economic risk"; in this subsection we proceed in that direction, establishing a link between our approach and network analysis.

A network (or graph) is a set of n nodes connected by edges. In an unweighted graph, the so-called *adjacency matrix* is an $n \times n$ matrix the entry (i,j) of which is one or zero according as nodes i and j are connected or not; in a weighted graph, that entry characterizes the strength of the connection between the two nodes. Diebold and Yilmaz (2014) point out that connectedness matrices are adjacency matrix of the weighted type[11] Two notable differences with Diebold and Yilmaz (2014), however, are that (i) our connectedness matrices are symmetric, hence the adjacency matrices of *undirected graphs*, and (ii) they are unconstrained, unlike those in Diebold and Yilmaz (2014), the rows of which sum up to one.

In the rest of this section, we apply to our long-run connectedness matrix some well-known techniques for similarity graphs.

4.1.1 Centrality

A very natural question in network analysis is to ask how "central", that is, how important, is each node in the whole system. This is clearly related to the total connectedness of a firm and resembles the widespread definition of systemically important financial institutions — namely, the firms which are considered to contribute more heavily to the systemic risk (see e.g. Acemoglu et al., 2015, and references therein).

A popular measure of centrality is the so-called *eigenvector centrality*: the centrality of a node i is defined as the corresponding element in the eigenvector associated with the largest eigenvalue of the adjacency matrix of a graph. As argued by Newman (2008), eigenvector centrality, in the analysis of weighted graphs, is a more appropriate concept of node centrality than the node's *degree* (i.e. the number of edges connected to a given node).

In the case of long-run connectedness, we will consider the adjacency matrix $\mathbf{Q}_{|\bullet|}(t,1)$ the entries of which are the absolute values of those in $\mathbf{Q}(t,1)$. In doing so, the link between two nodes i and j is unaffected by the sign of the covariance between X_{it} and X_{jt}. Furthermore, non-negative elements is a requirement for the application of the Perron-Frobenius theorem, granting the uniqueness of eigenvector centrality.

4.1.2 The graph Laplacian and its eigenvalues

Beyond centrality, other relevant concepts and techniques can be borrowed from network theory. Let us focus on the number of connected cross-sectional units, the strength of their connections, and how these evolve over time.

[11] Our connectedness matrices, as those in Diebold and Yilmaz (2014), have non-zero elements along the main diagonal. As pointed out by von Luxburg (2007), this is not a problem, since the Laplacian of a weighted graph does not depend on the strength of *self edges*.

In order to do so, we need the *Laplacian matrix* defined, at time t, as $\mathcal{L}(t) = \mathcal{D}(t) - \mathcal{A}(t)$, where $\mathcal{A}(t)$ is an adjacency matrix and $\mathcal{D}(t)$ the corresponding *degree matrix*. Inferring the number of connected units and the strength of their links requires focusing on the quantitatively most important connections. Following Diebold and Yilmaz (2014), consider percentiles in the (empirical) distribution of $\mathbf{Q}_{|\bullet|}(t,1)$'s entries, and replace those which are below a certain level with zeros: $\mathcal{A}(t)$ is the resulting matrix, the only non-zero elements of which are those related to sufficiently large entries of $\mathbf{Q}_{|\bullet|}(t,1)$. So doing, we are applying a technique for obtaining similarity graphs from distance measures known as *ε-neighborhood* for which the the adjacency matrix non-zero entries correspond to nodes whose mutual distance is above a certain threshold (von Luxburg, 2007).

Two important properties of the Laplacian matrix $\mathcal{L}(t)$ is that it is positive semi-definite, with eigenvalues containing all the information we are interested in; in particular,

(a) its smallest eigenvalue is equal to zero and its multiplicity represents the number of connected units in the graph (von Luxburg, 2007, Proposition 2);

(b) its smallest non-zero eigenvalue, often referred to as the *Fiedler number* (or *algebraic connectivity*) after the work of Fiedler (1973)[12] is a measure of the overall strength of connectedness in the graph.

5 Empirical results

5.1 Data and model specification

We applied the methodology described in the previous sections on a large datasets of daily stocks which have been constituents of the Standard & Poor 500 from December 31, 1999 to August 31, 2015; so doing we retain the daily maximum and minimum prices of $n = 329$ stocks observed over a sample of $T = 3939$ daily observations. Once their price ranges are calculated according to the definition of Parkinson (1980) in equation (1), we fit to the resulting panel the time-varying GDFM described in Sections 2 and 3 and apply the connectedness measures in Section 4.

The first step to the estimation of the GDFM is that of the spectral density matrix which, employing the estimator proposed by Neumann and von Sachs (1997) in equation (15), requires the choice of the smoothing kernels K and J in frequency and time domain, respectively, and their bandwidths h_T and b_T. For both kernels we used a triangular window, while the selected bandwidths are such that: $\lfloor h_T T/(2\pi) \rfloor = 5$, which corresponds to five frequencies and $\lfloor b_T T \rfloor = 10$ corresponding to ten days, i.e. two weeks, of trading. The time-kernel being two-sided, our results cannot be computed in real-time, but with a delay determined by the corresponding bandwidth: so, for example, our choice of b_T implies that in a predictive exercise our estimates would be available two weeks late.

Once the spectrum is estimated at each point in time, we need to determine the number of factors. The number q is estimated by applying the criterion of Hallin and Liška (2007) to the local estimate of the spectral density matrix defined in (15). Estimation at various points in time (various values of τ) supports evidence that $q = 3$ throughout the observation period,

[12] Fiedler numbers are also used in the construction of bi-partitioned graphs and related spectral clustering procedures: see Pothen et al. (1990).

hence is compatible with the assumption made of a "constant q".[13]

Finally, as spelled out in Section 3, in order to avoid the finite-sample dependence of the results on the cross-sectional ordering, we average results over 100 permutations of the observed panel. All the figures and tables shown below are related to the same Standard & Poor 500 dataset ($n = 329$, $T = 3939$).

5.2 Connectedness in the US (2000 – 2015)

Analyzing the evolution over time of our large (329×329) connectedness matrices requires some sort of cross-sectional aggregation. We begin with Figure 3, where we focus on cross-sectional distribution and norms. In the top panel we report the distribution of mean connectedness values $Q_i(t, z)$ for $i = 1, \ldots, n$ and, more precisely, their means, medians, 5-th, and 95-th percentiles. In the bottom panel, we plot the Frobenius norm of the connectedness matrices (other norms would be equally suitable, and actually yield very similar results). In all plots of Figure 3, connectedness is evaluated at instantaneous and long-run level, i.e. for $z = 0$ and $z = 1$.

Figure 3 shows that both long-run and instantaneous connectedness are spiking, quite dramatically, in conjunction with important financial crashes; this is particularly evident looking at the bottom panel where, for sake of comparison with the overall market performance, we are also plotting the daily values of the S&P 500 index. The turbulence at the beginning of our sample is related to a series of events starting with the burst of the Dot-com bubble early in 2000 and then followed by the 2002-2003 US recession — an event somehow related to other turmoils around the world like the previous recessions in East Asia, shortly followed by European and Japanese recessions — and the US stock market downturn of 2002. Connectedness stays low and stable all the time until 2007 and the onset of the global financial crisis, yielding the maximal connectedness values recorded in our sample.

Relatively quiet times have been overturned in the next few years, in relation to two major events. The first one is a rapid increase in connectedness in April 2010, just about a month before the "Flash crash" of May 6. A second abrupt connectedness increase is observed in 2011, some three weeks before the "Black Monday" of August 8, 2011. As stressed in the previous subsection, our bandwidth choice of ten business days (two weeks) in the time-domain smoother means that we could still foresee this spike in long-run connectedness one week before the occurrence of this dramatic event. In the same manner, we must remark that the link between estimated connectedness and the burst of the Dot-com bubble in March 2000 is less clear, since the large values of long-run connectedness we observe at the very beginning of our sample are followed by weeks of low connectedness before the turmoil takes place. Finally, the large drop of the S&P 500 in 2002 occurs less than two months after the increase in long-run connectedness which is still quite high towards the end of June 2002 before further market downturns. Albeit the development of an early warning system based on our connectedness measures goes beyond the goal of this paper, these preliminary findings suggest the pertinence of our analysis in real-time. We leave to future research a more systematic investigation in this direction.

Consistent with the view that financial risk is a forward looking concept affecting future investment strategies, a comparison of the two plots in the bottom panel of Figure 3 suggests that long-run connectedness is, quantitatively, the most relevant concept. Nevertheless, it

[13] Additional results under alternative penalty functions and related settings proposed by Hallin and Liška (2007) lead to the same conclusion. Furthermore, overestimating q has very little impact on qualitative results.

should be noticed that short-run dynamics also may reveal different patterns: see, for instance, the 2010 connectedness spike which, at instantaneous level, is even more pronounced than in the global financial crisis.

This impression is clearly confirmed when looking at the spectral connectedness results in Figure 4. Since spectral connectedness are normalized by the size of the frequency band considered, their scale allows for meaningful comparisons: we observe that connectedness becomes stronger and stronger as we get rid of high-frequency components. Once we only retain frequencies corresponding to cycles of at least one month, we obtain a connectedness which is very similar to the norm of long-run connectedness in Figure 3. By and large, the same picture is obtained if we restrict to the so-called business cycle frequencies (i.e., 4 to 32 quarters as in Baxter and King, 1999). We conclude that connectedness is somewhat stable at low to mid frequencies. Baruník and Křehlík (2018) find more heterogeneity over the spectrum of connectedness, but it is is hard to tell whether the difference is due to their low-dimensional vector autoregressive modeling approach and/or to the lack of time-variation in it.

One more confirmation of the big picture on the evolution of long-run connectedness — as seen in the two right plots of Figure 3 and in those plots of Figure 4 which filter out enough high frequencies — comes from the Fiedler number (as defined in Section 4.1.2) in Figure 7. Borrowed from network theory, that quantity measures the strength of the edges in our long-run connectedness graph, and in our data shows a strikingly similar evolution as in the aforementioned estimates of connectedness. The other plot in Figure 7 shows that the number of connected units increases in turmoil periods; a somewhat similar figure is obtained by Billio et al. (2012).[14]

Beyond their norms and their evolution over time, we also can observe connectedness matrices at few specific dates which have been selected in order to highlight differences. In Figure 5 and 6, we present heatmaps of the long-run and instantaneous connectedness matrices which, compared with those resulting from rolling covariances in Figure 2, reveal that connectedness in the long-run absorbs, or arguably even amplifies, the time-variation in the data while the short-run is relatively smoother over time.

5.3 Connectedness during the great crisis (2007–2009)

Going back to the right-hand plots of Figure 3, we observe that the highest value in long-run connectedness corresponds with the onset of the crisis; its magnitude, moreover, is quite large relatively to other peaks. Figure 8 essentially zooms into the same plots with added dashed lines for the 99-th percentiles of the solid lines plotted in their time-series distributions from the beginning of the sample to November 15, 2006 (the starting point of the crisis subsample we now focus on); so doing, we are setting a benchmark to relatively rare outcomes and we can observe their path in a more convenient scale.

The largest value observed in the norm of the long-run connectedness matrix is dated October 26, 2008, shortly after the bankruptcy of Lehman Brothers (September 15, 2008) and well before the minimum of the S&P 500 index during the March 9, 2009 bear market of 2007-2009: in this time span the index continued to drop, recording an overall decrease of about 30-percent. The norm of the long-run connectedness matrix starts to reach relatively high levels already during 2007. The 99-th percentile benchmark is almost continuously violated

[14]Both plots in Figure 7 are quite stable to sufficiently large choices of the percentile chosen for the ε-neighborhood technique described in Section 4.1.2.

in this subsample starting from as early as November 2006; the maximum norm of long-run connectedness we estimate in December 2007 is about four time as large as the 99-th percentile of its distribution until November 15, 2006. Several spikes in long-run connectedness are observed during 2007. In late January 2007, long-run connectedness abruptly jumps to about 20 times its 99-th percentile, and, between August and September 2007, quite consistently up to 30 times that same percentile. Finally, in the third week of December 2007, long-run connectedness has a spectacular increase and does not revert for about three months; during this stint, the long-run connectedness norm reaches its third largest value since the beginning of our observation period. The maximal value — a spike in 2000 due to the burst of the Dot-com bubble — is overcome in August 2008, after about three months of apparent calm in which the market performed well. The mid-July 2008 connectedness increase is overwhelming until about 6-7 weeks before March 9, 2009, when the S&P 500 eventually exhibits a turning point and starts recovering.

All in all, the same picture arises from the distribution in the top panel of Figure 8, and we must conclude that long-run connectedness was consistently experiencing a series of quite rare events as early as 2007. For sake of comparison, the TED spread — a prominent measure of perceived credit-risk — started to increase in August 2007, reaching its maximum between September and October 2008. For a more narrative account of how the crisis affected the US market and individual industries, we refer to the next section where connectedness is analysed at a finer, sectoral, scale.

5.4 Sectoral evidence

Another sensible way to aggregate our results consists in taking into account the industrial sectors of the stocks in our panel. In Figure 9 we consider the evolution over time of connectedness within the main industry-specific sectors, as defined in equation (27). Sector-specific connectedness essentially is an average total connectedness within the sector. Plotting the differences between industry-specific connectedness and the panel-wide average total connectedness provides (for long-run connectedness) interesting insights into the heterogeneity of dynamics across the various sectors. This tells us whether the long-run connectedness in any given sector comoves with that in the market exceeding, subceeding or remaining in lockstep with it.

Probably unsurprisingly in hindsight, during the great financial crisis the connectednesses of Banks, Financial Services, Real Estate and Investment Trusts, Life Insurance are the largest. Also affected by the great crisis above and beyond the market average are the Electricity, Construction and Materials, Oil and Gas Producers, and to a lesser extent, Oil Equipment and Services, and Nonlife Insurance sectors. A number of sectors display by and large the same amount of connectedness as the market average; these are Aerospace and Defense, Chemicals, Electronic and Electrical Equipment, General Retailers, Health Care Equipment and Services, Support Services. The sectors weathering the storm in connectenedness as compared with the average connectedness in the market are Food and Drug Retailers, Food Producers, Media, Pharmaceuticals and Biotechnology, Software and Computer Services, Tobacco, Technology, Hardware and Equipment.

Some sectors, quite closely related one each other, used to move in lockstep with the market in the first half of our sample until the great crisis, then break apart afterwards; this is the case of Household Goods and Home Construction, Industrial Engineering, Industrial Metals, an Mining, Industrial Transportation, General Industrials, General Retailers,

Forestry, and Paper.

The turmoils of early 2000's are associated with high connectedness in some sectors which are clearly related to the Dot-com bubble (Software and Computer Services, Technology Hardware and Equipment, Media, Fixed Line Telecommunications) together with more "traditional" sectors (Electricity, Banks).

Two more results should be stressed from a broader observation of Figure 9 beyond the crisis of 2007–2009. First, the heterogeneity we find across sectors is much less in calm times than during financial turmoils. Second, the long-run connectedness norms of Banks, Financial Services and Real Estate Investment Trusts are spiking higher than any other sector during the most severe turmoils.

The pattern of average sectoral eigenvector centrality in Figure 10 shows that the most central nodes belong in sectors where long-run connectedness is high.[15] All in all, this figure is indeed consistent with the results on sectoral connectedness previously discussed.

Finally, Table 1 is listing the firms associated with the most central nodes at the same selected dates as in previously commented figures. There is strong evidence that centrality dynamics have a sectoral flavour. In fact, at many of these selected dates, the most central nodes belong to a few sectors: for example, while on April 27, 2000 most of the nodes in the highest percentiles of the centrality distribution belong to Technology, Hardware and Equipment, the same applies on October 30, 2008 to firms in Real Estate Investment Trusts.

A more focused investigation into such sectoral dynamics combining structural, economic, identification with the block-structure of the industrial sectors in the spirit of Barigozzi et al. (2018) goes beyond the goal of this paper. Nevertheless, it should be noticed that the common factors possibly do have a locally pervasive effect in our panel of price ranges. Although our time-varying GDFM (2) does not include any modeling of group-factor structure, we are imposing no restriction against this form of cross-sectional dependence, and the decomposition of connectedness measures into a sum of q orthogonal factor-specific contributions sheds some light into that direction. In Figure 11, we show heatmaps of such decompositions — as defined in equation (25) — applied to the long-run connectedness matrix. Inspection of that figure indicates that, indeed, some factors might, at least temporarily, have a sectoral connotation (as, e.g. , the second factor in April 27, 2000, the third factor in February 14, 2008, the first and second factors in October 16, 2014, etc.).

6 Conclusions

We propose a novel method for the analysis of financial connectedness which, unlike that of Diebold and Yilmaz (2014), is adequate for large datasets where episodes of systemic risk are typically pervasive. Furthermore, allowing for time-varying parameters, our model is better suited for the analysis of risk dynamics. Our method relies on a time-varying version of the so-called General Dynamic Factor Model which is specifically designed for the analysis of high-dimensional locally stationary processes in the sense of Dahlhaus (2009, 1997), and extends previous work on dynamic factor models (especially recent results in Forni et al., 2015, 2017) by allowing for time-varying loading filters and time-varying spectra. Thus, we contribute to the recent, and rapidly growing, literature on non-stationary factor models (see Mikkelsen et al., 2018; Su and Wang, 2017; Bates et al., 2013; Motta et al., 2011; Del Negro

[15] In Appendix we show centrality disaggregated $n \times T$ heatmaps for each individual firm, which exhibit similar dynamics.

and Otrok, 2008, among others) which, so far is dominated by time-varying factor models of the static type (i.e., based on scalar factor loadings).

Our method indicates that the comovements in a high-dimensional dataset of daily price ranges of constituents of the Standard & Poor 500 index are remarkably strong; this suggests basing the analysis of connectedness on (estimators of) the impulse response functions with respect to common factors or shocks — a straightforward source of systemic risk also considered by Billio et al. (2012). In the empirical part of this work, we show that large increases in connectedness — especially in their mid to low frequencies — are associated with the most important turmoils in the stock market. Connectedness does not span all industrial sectors in the same way and, especially during the turmoils of 2007–2009, Banks and, more generally, firms in the financial sector had prevalent roles. Nevertheless, sectoral connectedness heterogeneity is found to decrease in the more recent part of our sample, after the great crisis.

Two important questions are left for future research. First, we noticed how increasing connectedness is associated with serious market downturns, often anticipating them; it seems natural, thus, to develop an early warning system based on our connectedness measures and investigate its performance. Second, a structural analysis along the lines of Barigozzi et al. (2018) — but based our novel time-varying framework — would allow us to attach an economic meaning to each individual common shock and shed more light on the sources of connectedness and their propagation mechanisms.

References

Acemoglu, D., A. Ozdaglar, and A. Tahbaz-Salehi (2010). Cascades in Networks and Aggregate Volatility. Working Paper 16516, National Bureau of Economic Research.

Acemoglu, D., A. Ozdaglar, and A. Tahbaz-Salehi (2015). Systemic Risk and Stability in Financial Networks. *The American Economic Review 105*(2), 564–608.

Acharya, V., R. Engle, and M. Richardson (2012). Capital Shortfall: A New Approach to Ranking and Regulating Systemic Risks. *American Economic Review 102*(3), 59–64.

Acharya, V. V., L. H. Pedersen, T. Philippon, and M. Richardson (2017). Measuring Systemic Risk. *The Review of Financial Studies 30*(1), 2–47.

Adrian, T. and M. K. Brunnermeier (2016). CoVaR. *American Economic Review 106*(7), 1705–1741.

Alizadeh, S., M. W. Brandt, and F. X. Diebold (2002). Range-Based Estimation of Stochastic Volatility Models. *The Journal of Finance 57*(3), 1047–1091.

Allen, F., A. Babus, and E. Carletti (2012). Asset commonality, debt maturity and systemic risk. *Journal of Financial Economics 104*(3), 519–534.

Anderson, B. D. and M. Deistler (2008a). Generalized linear dynamic factor models-A structure theory. In *Proceedings of the 47th IEEE Conference on Decision and Control*, pp. 1980–1985.

Anderson, B. D. and M. Deistler (2008b). Properties of zero-free transfer function matrices. *SICE Journal of Control, Measurement and System Integration 1*, 284–292.

Bai, J. and S. Ng (2002). Determining the Number of Factors in Approximate Factor Models. *Econometrica 70*(1), 191–221.

Balke, N. S. and M. E. Wohar (2002). Low-Frequency Movements in Stock Prices: A State-Space Decomposition. *The Review of Economics and Statistics 84*(4), 649–667.

Bandi, F. M. and A. Tamoni (2017). The Horizon of Systematic Risk: A New Beta Representation. SSRN Scholarly Paper ID 2337973, Rochester, NY.

Barigozzi, M., H. Cho, and P. Fryzlewicz (2018). Simultaneous multiple change-point and factor analysis for high-dimensional time series. *Journal of Econometrics 206*, 187–225.

Barigozzi, M. and M. Hallin (2017). A network analysis of the volatility of high dimensional financial series. *Journal of the Royal Statistical Society: Series C (Applied Statistics) 66*(3), 581–605.

Barigozzi, M., M. Hallin, and S. Soccorsi (2018). Identification of Global and Local Shocks in International Financial Markets via General Dynamic Factor Models. *Journal of Financial Econometrics 33*, 625–642.

Barrero, J. M., N. Bloom, and I. Wright (2017). Short and Long Run Uncertainty. Working Paper 23676, National Bureau of Economic Research.

Baruník, J. and T. Křehlík (2018). Measuring the Frequency Dynamics of Financial Connectedness and Systemic Risk. *Journal of Financial Econometrics 16*, 271–296.

Bates, B. J., M. Plagborg-Møller, J. H. Stock, and M. W. Watson (2013). Consistent factor estimation in dynamic factor models with structural instability. *Journal of Econometrics 177*(2), 289–304.

Baxter, M. and R. G. King (1999). Measuring Business Cycles: Approximate Band-Pass Filters for Economic Time Series. *The Review of Economics and Statistics 81*(4), 575–593.

Benoit, S., J.-E. Colliard, C. Hurlin, and C. Pérignon (2017). Where the Risks Lie: A Survey on Systemic Risk. *Review of Finance 21*(1), 109–152.

Billio, M., M. Getmansky, A. W. Lo, and L. Pelizzon (2012). Econometric measures of connectedness and systemic risk in the finance and insurance sectors. *Journal of Financial Economics 104*(3), 535–559.

Brockwell, P. J. and R. A. Davis (1991). *Time Series: Theory and Methods* (2 ed.). Springer Series in Statistics. New York: Springer-Verlag.

Brownlees, C. and R. F. Engle (2017). SRISK: A Conditional Capital Shortfall Measure of Systemic Risk. *The Review of Financial Studies 30*(1), 48–79.

Brownlees, C. T. and G. M. Gallo (2010). Comparison of Volatility Measures: a Risk Management Perspective. *Journal of Financial Econometrics 8*(1), 29–56.

Dahlhaus, R. (1997). Fitting time series models to nonstationary processes. *The Annals of Statistics 25*(1), 1–37.

Dahlhaus, R. (2009). Local inference for locally stationary time series based on the empirical spectral measure. *Journal of Econometrics 151*(2), 101–112.

Del Negro, M. and C. Otrok (2008). Dynamic Factor Models with Time-Varying Parameters: Measuring Changes in International Business Cycles. SSRN Scholarly Paper ID 1136163, Rochester, NY.

Dew-Becker, I. and S. Giglio (2016). Asset Pricing in the Frequency Domain: Theory and Empirics. *The Review of Financial Studies 29*(8), 2029–2068.

Diebold, F. X. and K. Yilmaz (2014). On the network topology of variance decompositions: Measuring the connectedness of financial firms. *Journal of Econometrics 182*(1), 119–134.

Eichler, M., G. Motta, and R. von Sachs (2011). Fitting dynamic factor models to non-stationary time series. *Journal of Econometrics 163*(1), 51–70.

Engle, R. F. (2010). The Risk that Risk Will Change. SSRN Scholarly Paper ID 1539166, Rochester, NY.

Fiedler, M. (1973). Algebraic connectivity of graphs. *Czechoslovak Mathematical Journal 23*(98), 298–305.

Forni, M., D. Giannone, M. Lippi, and L. Reichlin (2009). Opening the black box: Structural factor models with large cross sections. *Econometric Theory 25*(5), 1319–1347.

Forni, M., A. Giovannelli, M. Lippi, and S. Soccorsi (2018). Dynamic factor model with infinite-dimensional factor space: Forecasting. *Journal of Applied Econometrics 33*(5), 625–642.

Forni, M., M. Hallin, M. Lippi, and L. Reichlin (2000). The generalized dynamic-factor model: Identification and estimation. *Review of Economics and Statistics 82*(4), 540–554.

Forni, M., M. Hallin, M. Lippi, and P. Zaffaroni (2015). Dynamic factor models with infinite-dimensional factor spaces: One-sided representations. *Journal of Econometrics 185*(2), 359–371.

Forni, M., M. Hallin, M. Lippi, and P. Zaffaroni (2017). Dynamic factor models with infinite-dimensional factor spaces: Asymptotic analysis. *Journal of Econometrics 199*(1), 74–92.

Hallin, M. and M. Lippi (2013). Factor models in high-dimensional time seriesâĂŤA time-domain approach. *Stochastic Processes and their Applications 123*(7), 2678–2695.

Hallin, M. and R. Liška (2007). Determining the Number of Factors in the General Dynamic Factor Model. *Journal of the American Statistical Association 102*(478), 603–617.

Korobilis, D. and K. Yilmaz (2018). Measuring Dynamic Connectedness with Large Bayesian VAR Models. SSRN Scholarly Paper ID 3099725, Rochester, NY.

Mikkelsen, J. G., E. Hillebrand, and G. Urga (2018). Consistent estimation of time-varying loadings in high-dimensional factor models. *Journal of Econometrics 208*(2), 535–562.

Motta, G., C. M. Hafner, and R. von Sachs (2011). Locally stationary factor models: Identification and nonparametric estimation. *Econometric Theory 27*(6), 1279–1319.

Neumann, M. H. and R. von Sachs (1997). Wavelet thresholding in anisotropic function classes and application to adaptive estimation of evolutionary spectra. *The Annals of Statistics 25*(1), 38–76.

Newman, M. E. (2008). The mathematics of networks. *The new palgrave encyclopedia of economics 2*(2008), 1–12.

Ortu, F., A. Tamoni, and C. Tebaldi (2013). Long-Run Risk and the Persistence of Consumption Shocks. *The Review of Financial Studies 26*(11), 2876–2915.

Parkinson, M. (1980). The Extreme Value Method for Estimating the Variance of the Rate of Return. *The Journal of Business 53*(1), 61–65.

Pothen, A., H. D. Simon, and K.-P. Liou (1990). Partitioning sparse matrices with eigenvectors of graphs. *SIAM journal on matrix analysis and applications 11*(3), 430–452.

Rodríguez-Poo, J. M. and O. Linton (2001). Nonparametric factor analysis of residual time series. *Test 10*(1), 161–182.

Stock, J. H. and M. W. Watson (2002). Forecasting Using Principal Components From a Large Number of Predictors. *Journal of the American Statistical Association 97*(460), 1167–1179.

Su, L. and X. Wang (2017). On time-varying factor models: Estimation and testing. *Journal of Econometrics 198*(1), 84–101.

Vershynin, R. (2018). *High dimensional probability. An introduction with applications in Data Science*. Cambridge University Press.

von Luxburg, U. (2007). A tutorial on spectral clustering. *Statistics and Computing 17*(4), 395–416.

Figure 1: Share of variance explained by dynamic eigenvalues in the S&P500 panel of log ranges

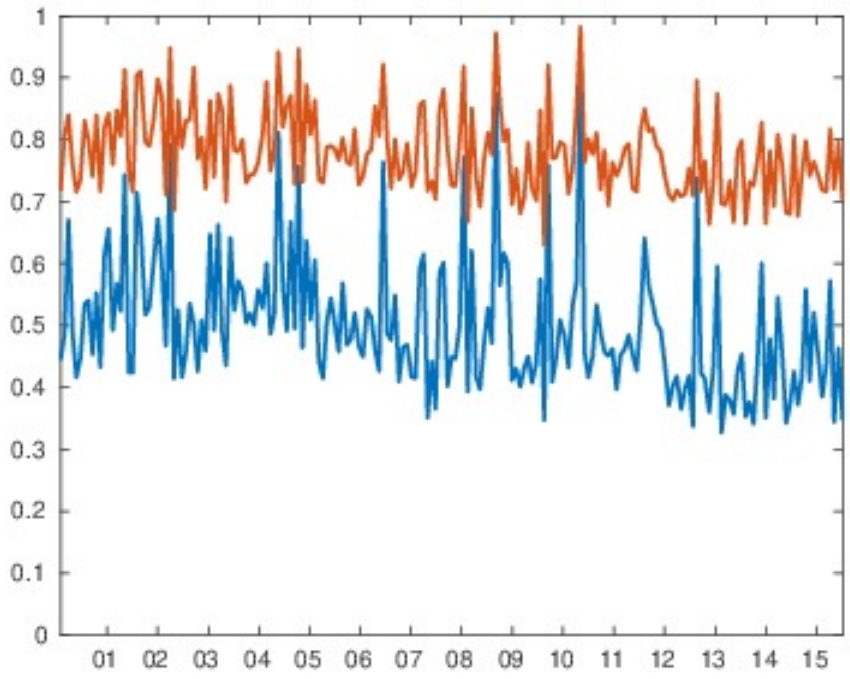

Time series of estimated shares of variance accounted for by the first factor (blue line) and the first three factors (red line). The share of variance explained at time t by the first k factors is defined as

$$\frac{\sum_{j=1}^{k}\sum_{h=1}^{T}\widehat{\lambda}_{j;n,T}\left(t/T;\theta_\ell\right)}{\sum_{j=1}^{n}\sum_{h=1}^{T}\widehat{\lambda}_{j;n,T}\left(t/T;\theta_\ell\right)},\quad \theta_\ell=2\pi h_T\ell,\ \ell=1,\ldots,\lfloor 1/h_T\rfloor$$

where $\widehat{\lambda}_{j;n,T}\left(t/T;\theta_\ell\right)$ is the jth largest eigenvalue of $\widehat{\mathbf{\Sigma}}^{X}_{n,T}\left(t/T,\theta_\ell\right)$ defined in (15).

Figure 2: Covariance matrix at selected dates

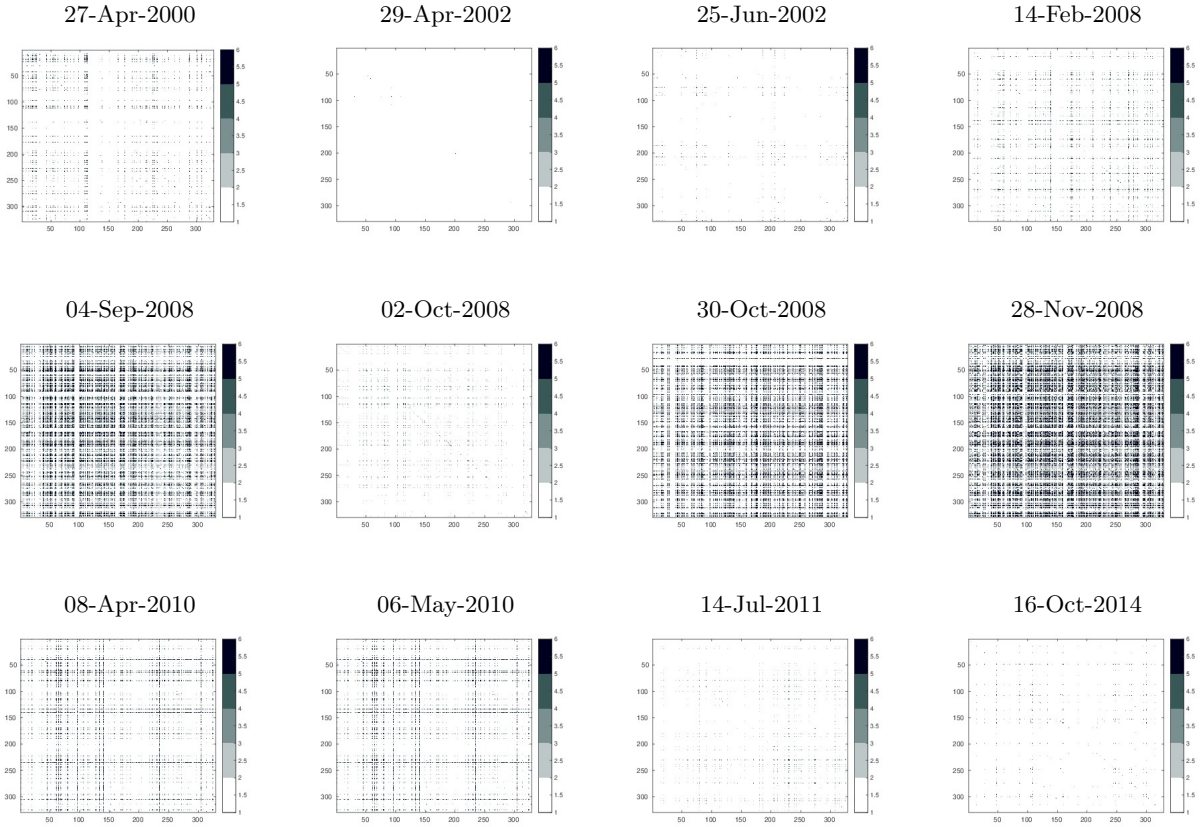

Rolling estimates of the sample covariance matrix using a triangular kernel.

Figure 3: INSTANTANEOUS AND LONG-RUN CONNECTEDNESS

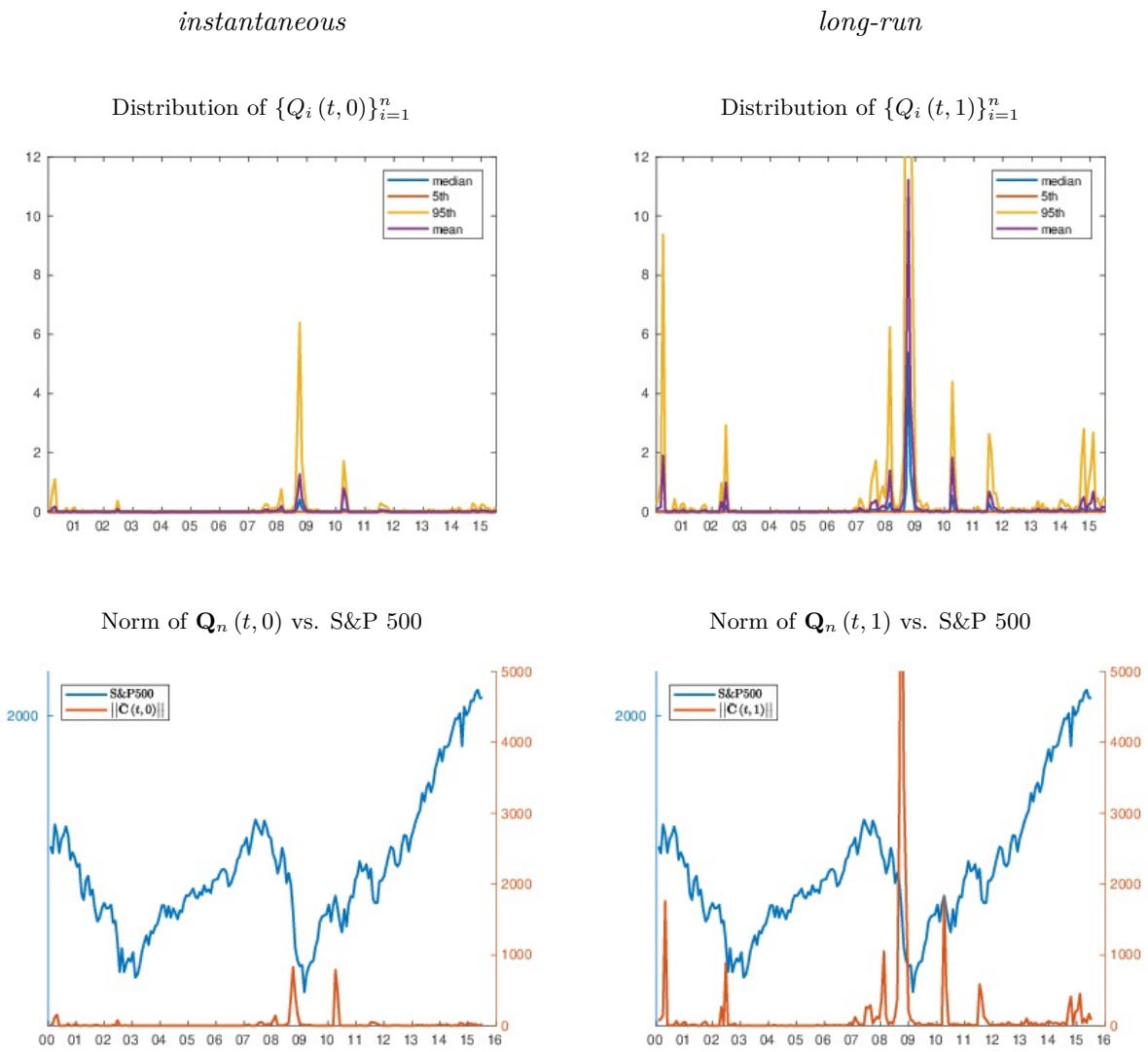

Top panel: mean, median, 5-th and 95-th percentiles of the distribution of mean instantaneous (left plots) and long-run (right plots) connectedness $Q_i(t,0)$, $Q_i(t,1)$, for $i = 1, \ldots, n$ as indicated in the legend. Bottom panel: Frobenius norms of the instantaneous and long-run connectedness matrices plotted together with the S&P 500 index, as indicated in the legend.

Figure 4: NORM OF SPECTRAL CONNECTEDNESS MATRICES $\mathbf{Q}_{\Theta;n}(t)$

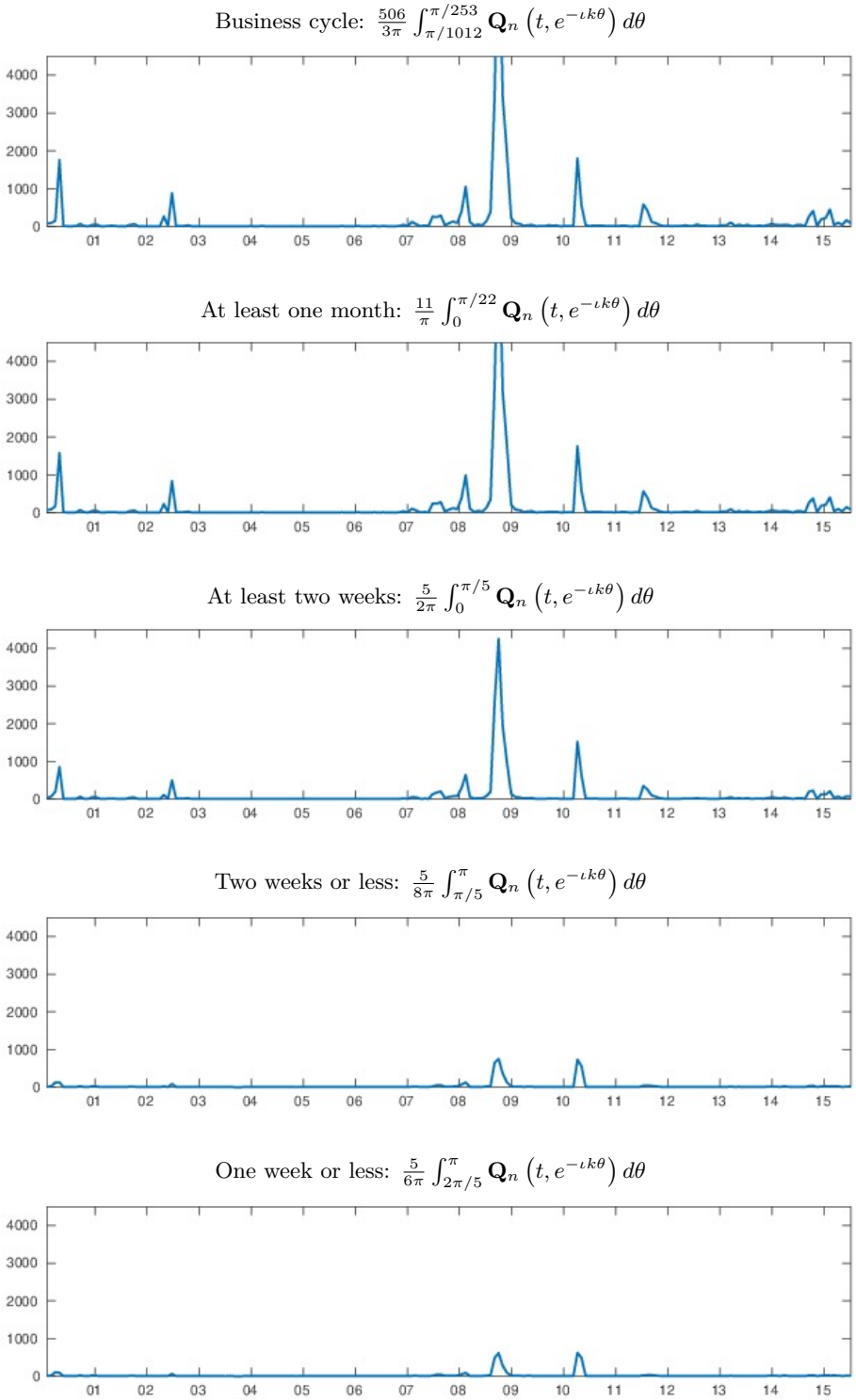

Time series of the Frobenius norm of the spectral connectedness matrices evaluated for different frequency bands. Over each plot the period of the frequencies in the band considered and the formula for the corresponding connectedness matrix are indicated. Business cycle frequencies correspond to cycles between 4 and 32 quarters.

Figure 5: HEATMAPS OF LONG-RUN CONNECTEDNESS, $\mathbf{Q}_n(t,1)$, AT SELECTED DATES

27-Apr-2000

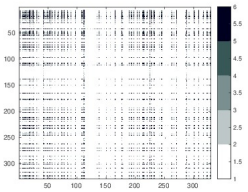

29-Apr-2002

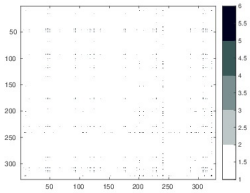

25-Jun-2002

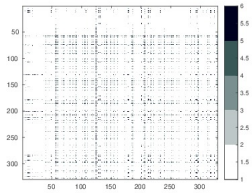

14-Feb-2008

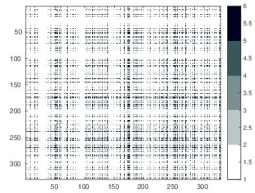

04-Sep-2008

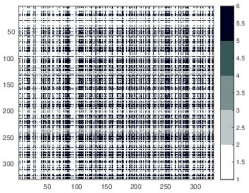

02-Oct-2008

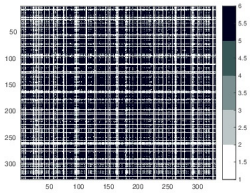

30-Oct-2008

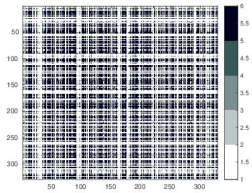

28-Nov-2008

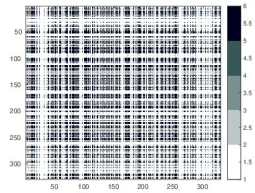

08-Apr-2010

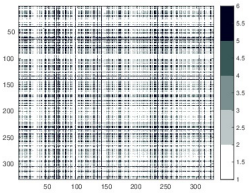

06-May-2010

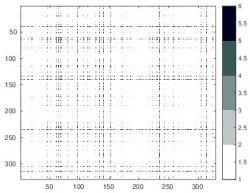

14-Jul-2011

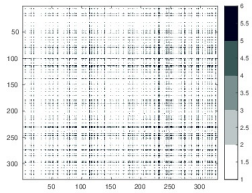

16-Oct-2014

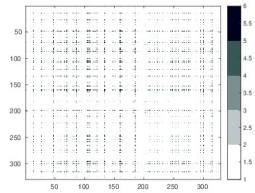

Figure 6: Heatmaps of instantaneous connectedness $\mathbf{Q}_n(t,0)$ at selected dates

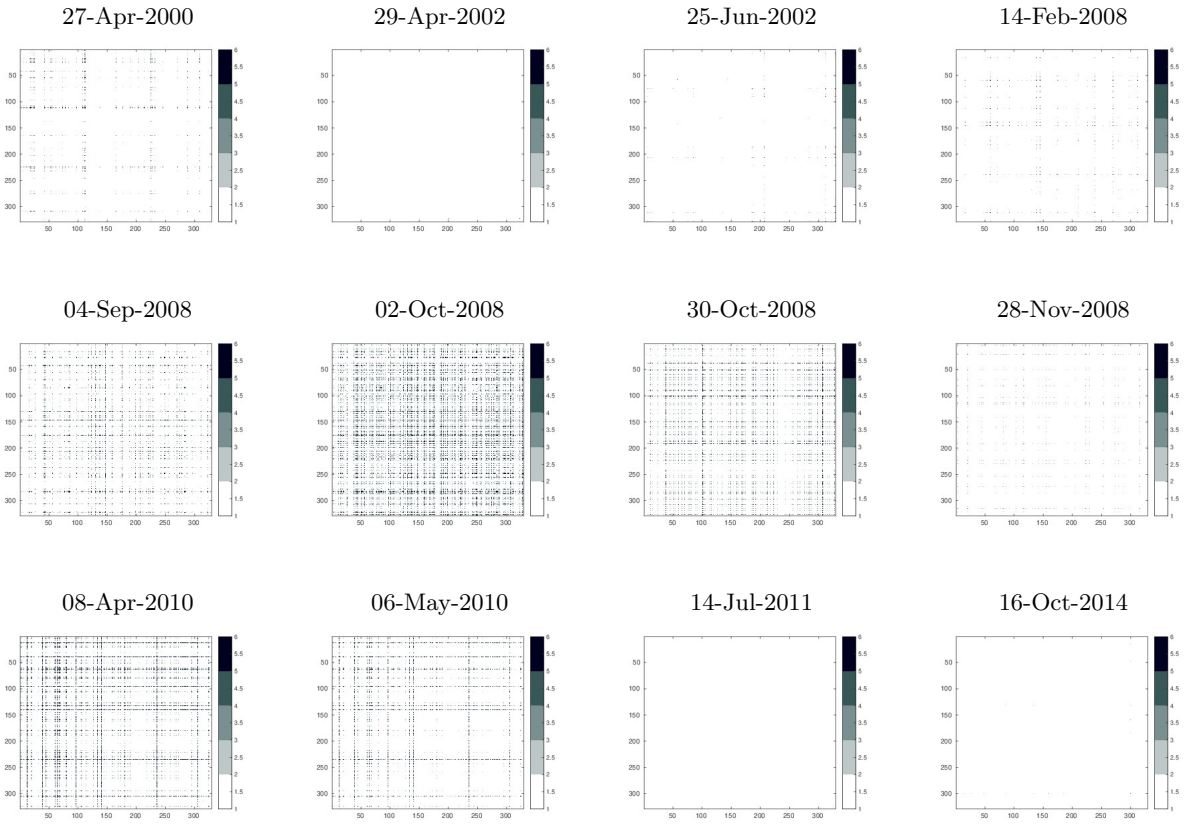

Figure 7: Fiedler number and connected nodes in long-run connectedness

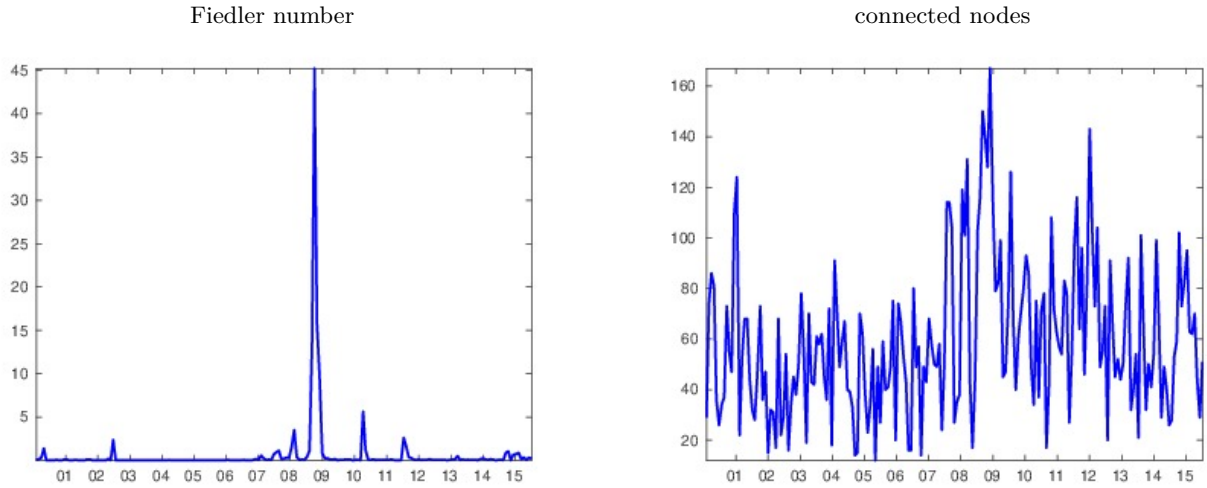

Figure 8: Long-run connectednness during the great financial crisis.

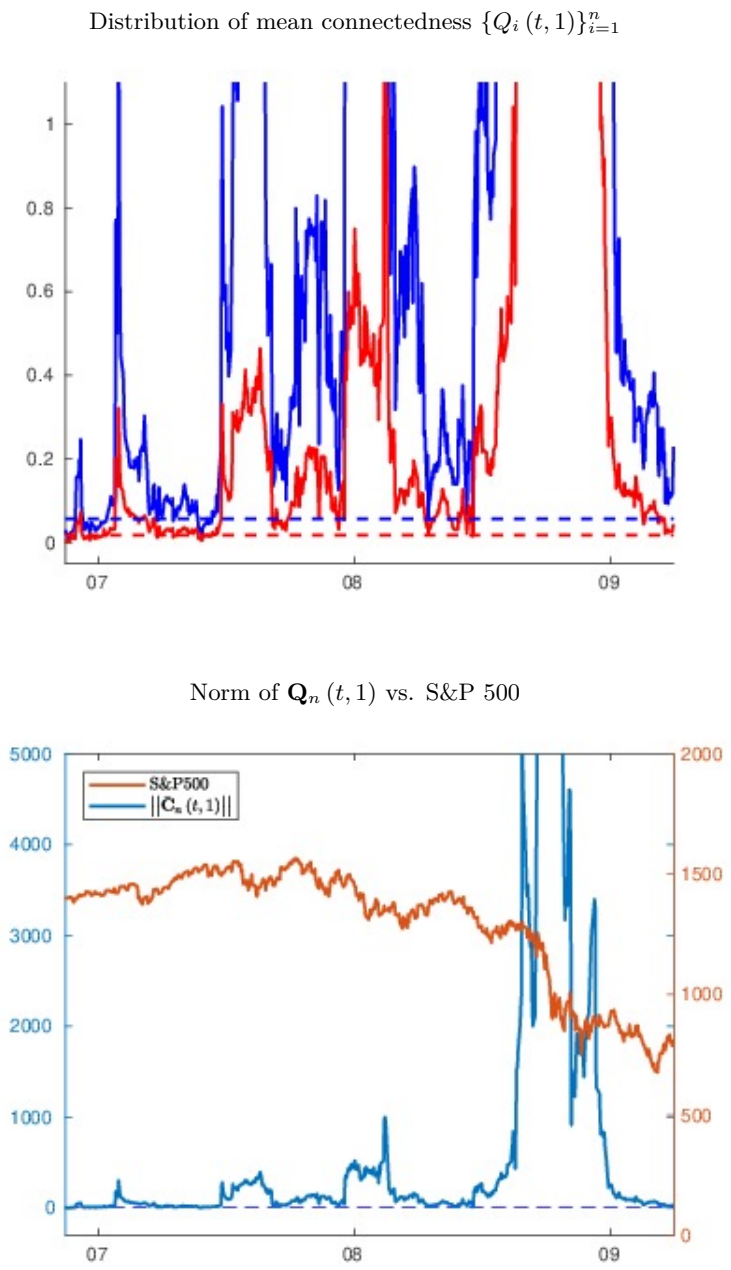

Top plot: the solid lines represent the 95-th percentile and the average, respectively, of the cross-sectional distribution of the mean connectedness values $Q_i(t,1)$ for $i = 1, \ldots, n$ at any given t, while the dashed lines represent the 99-th percentiles of their own time series distributions in the subsample running from January 4, 2000 to November 15, 2006. Bottom plot: the solid line is the time series of the Frobenius norm of $\mathbf{Q}_n(t,1)$ while the dashed line is its 99-th percentile in the subsample running from January 4, 2000 to November 15, 2006.

Figure 9: Sectoral long-run connectedness

Aerospace and Defense

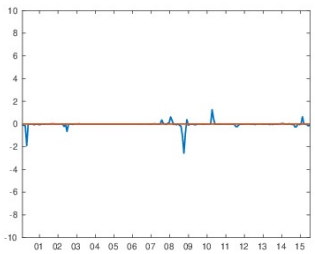

Automobiles and Parts

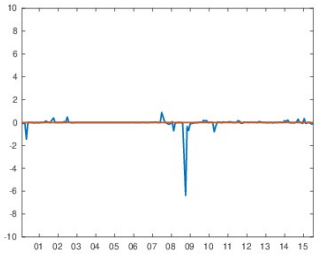

Banks

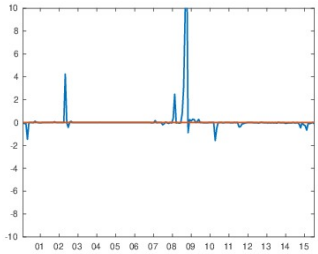

Beverages

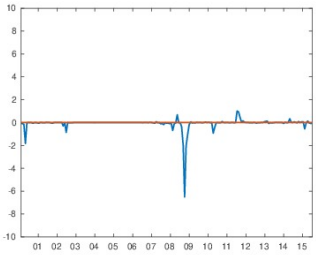

Chemicals

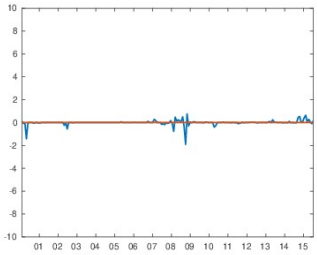

Construction and Materials

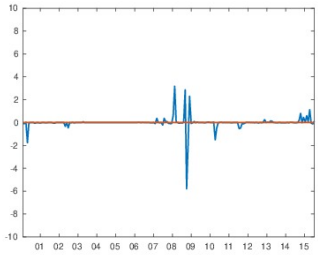

Electricity

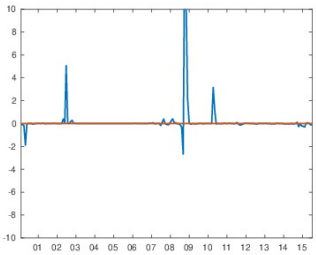

Electronic and Electrical Equip.

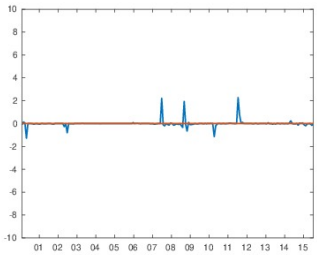

Financial Services (Sector)

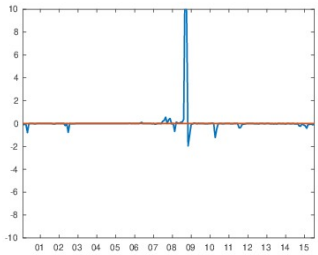

Fixed Line Telecommunications

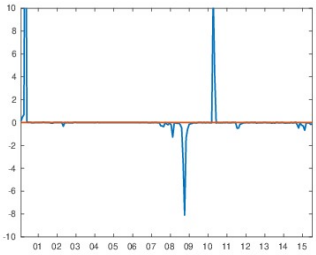

Food Producers

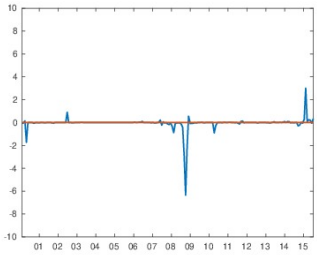

Food and Drug Retailers

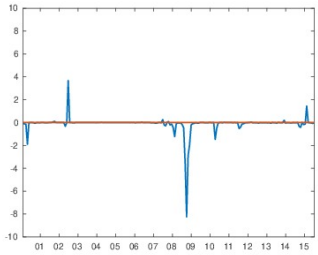

Forestry and Paper

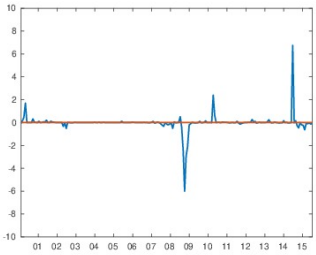

Gas, Water and Multiutilities

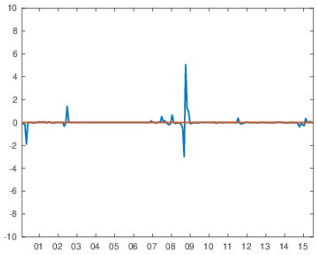

General Industrials

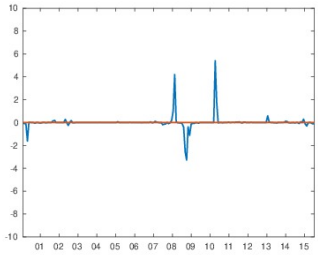

- Continued on next page -

Figure 9 – continued from previous page

General Retailers

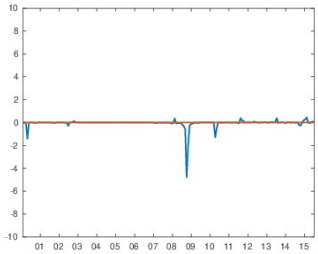

Health Care Equip. and Services

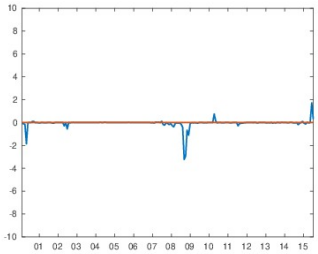

Household Goods and Home Constr.

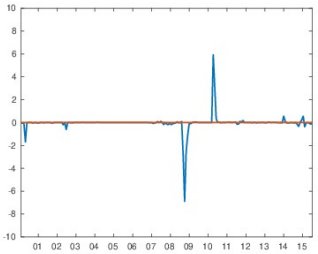

Industrial Engineering

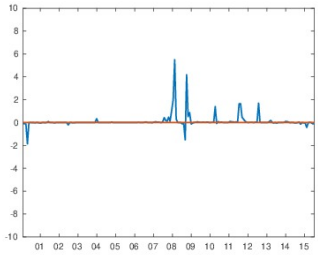

Industrial Metals and Mining

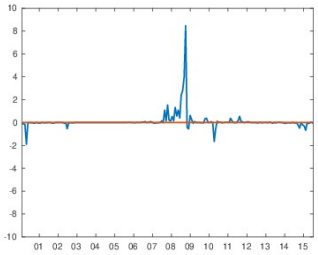

Industrial Transportation

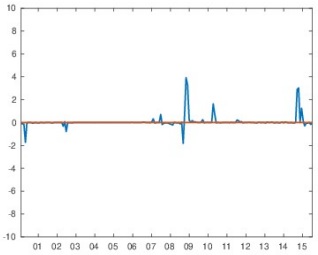

Leisure Goods

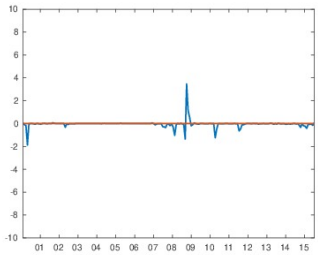

Life Insurance

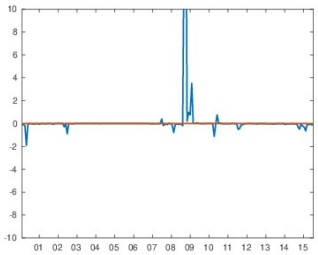

Media

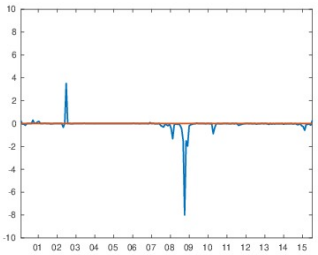

Nonlife Insurance

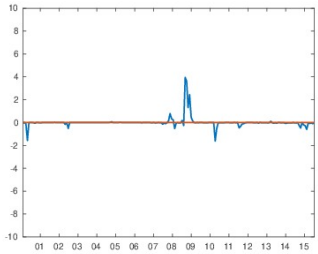

Oil Equip. and Services

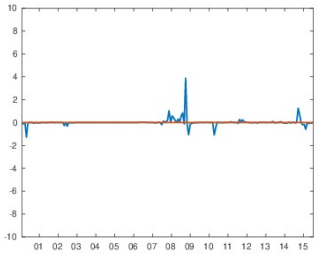

Oil and Gas Producers

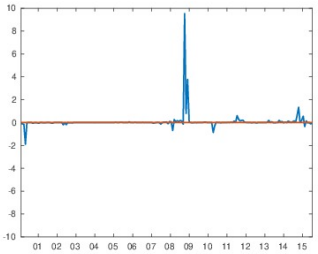

Personal Goods

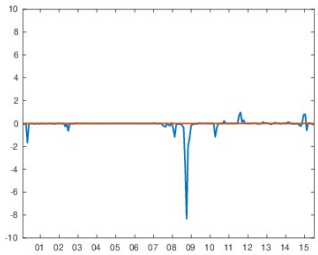

Pharmaceuticals and Biotech.

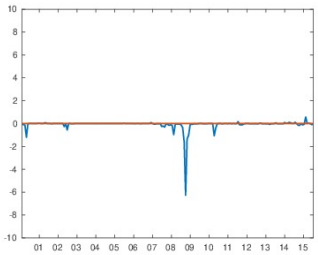

Real Estate Investment Trusts

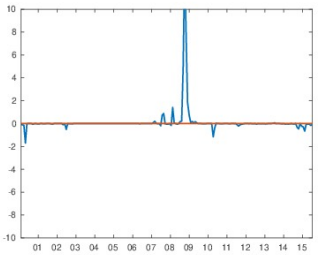

- Continued on next page -

Figure 9 – continued from previous page

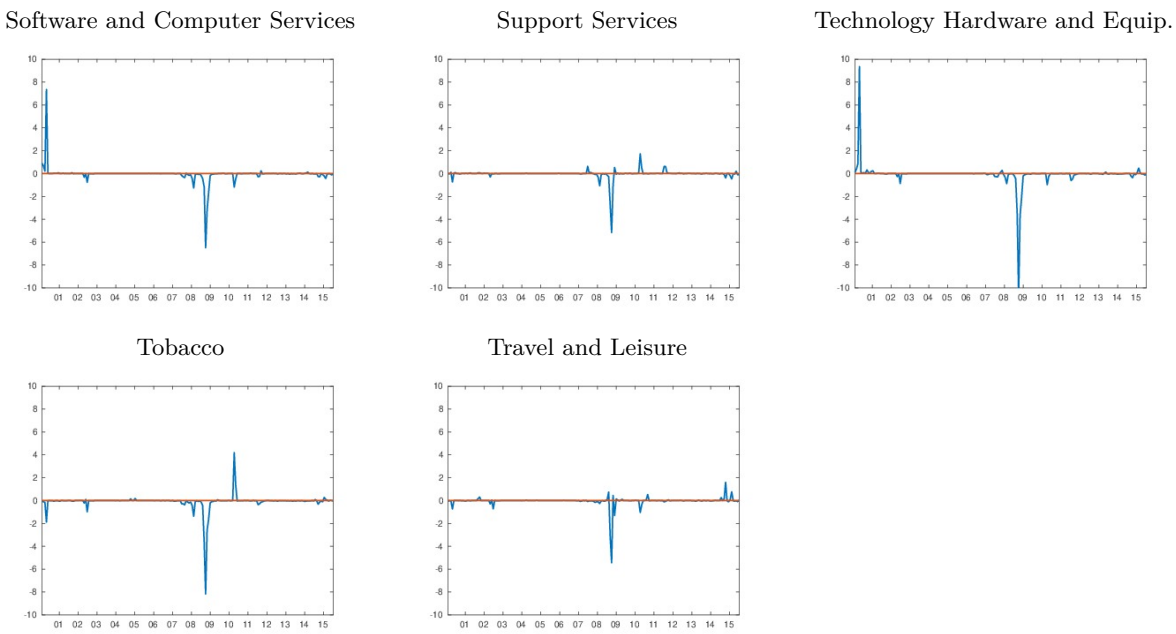

Blue lines are differences between the sectoral means $\mathbf{Q}_{[\mathcal{S}(k),\bullet]}(t,1)$ for the sectors under reference and the mean value across all firms. Red lines correspond to the zero value where sectoral mean equals the overall mean.

Figure 10: Eigenvector centrality in long-run connectedness at sectoral level

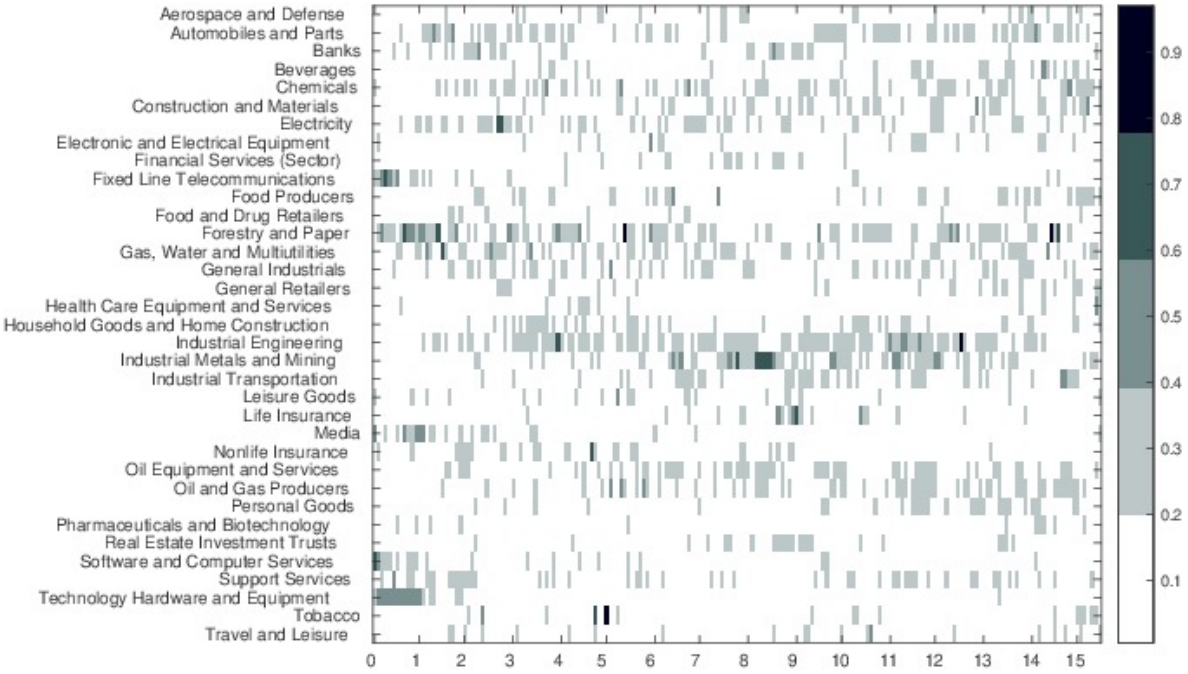

At each point in time (years in abscissa), the centrality in the long-run connectedness newtork of each industrial sector (in ordinate) is the corresponding element of the eigenvector associated with the largest eigenvalue of a matrix whose generic entry is the sector-specific long-run connectedness $\mathbf{Q}_{[\mathcal{S}(k),\bullet]}(t,1)$ defined in equation (27).

Figure 11: Heatmaps of sectoral long-run connectedness matrices decomposed by factor at selected dates.

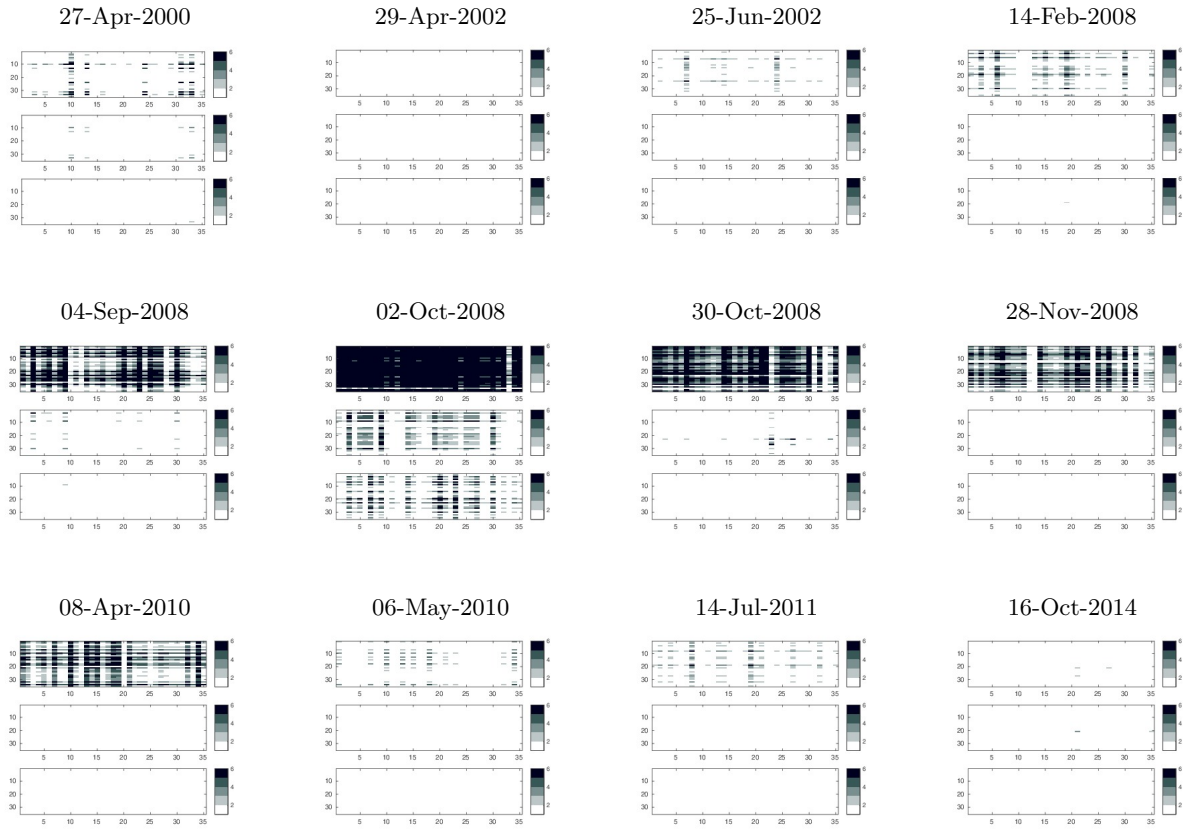

Heatmaps of the sectoral long-run connectedness matrices decomposed by the contribution of the first three factors. These matrices relate to the selected dates indicated on the top of each heatmap.

Table 1: Eigenvector centrality in long-run connectedness

27-Apr-2000	
99-th percerntile	
YAHOO	Software and Computer Services
LEVEL 3 COMMS.	Fixed Line Telecommunications
SANDISK	Technology Hardware and Equipment
95-th percerntile	
ORACLE	Software and Computer Services
INTERNATIONAL BUS.MCHS.	Software and Computer Services
INTEL	Technology Hardware and Equipment
CISCO SYSTEMS	Technology Hardware and Equipment
QUALCOMM	Technology Hardware and Equipment
PRICELINE GROUP	Travel and Leisure
BROADCOM A	Technology Hardware and Equipment
CORNING	Technology Hardware and Equipment
APPLIED MATS.	Technology Hardware and Equipment
MOTOROLA SOLUTIONS	Technology Hardware and Equipment
RED HAT	Software and Computer Services
CITRIX SYS.	Software and Computer Services
XILINX	Technology Hardware and Equipment
29-Apr-2002	
99-th percerntile	
XCEL ENERGY	Electricity
REGIONS FINL.NEW	Banks
HUNTINGTON BCSH.	Banks
95-th percerntile	
PFIZER	Pharmaceuticals and Biotechnology
HONEYWELL INTL.	General Industrials
US BANCORP	Banks
AMERICAN TOWER	Real Estate Investment Trusts
ANADARKO PETROLEUM	Oil and Gas Producers
ARCHER-DANLS.-MIDL.	Food Producers
PPG INDUSTRIES	Chemicals
APPLIED MATS.	Technology Hardware and Equipment
XCEL ENERGY	Electricity
HERSHEY	Food Producers
ROCKWELL AUTOMATION	Industrial Engineering
REGIONS FINL.NEW	Banks
TIFFANY & CO	General Retailers
BALL	General Industrials
GOODYEAR TIRE & RUB.	Automobiles and Parts
HUNTINGTON BCSH.	Banks
25-Jun-2002	
99-th percerntile	
CARDINAL HEALTH	Food and Drug Retailers
XCEL ENERGY	Electricity
OMNICOM GROUP	Media
95-th percerntile	
FORD MOTOR	Automobiles and Parts
TJX	General Retailers
ARCHER-DANLS.-MIDL.	Food Producers
AMER.ELEC.PWR.	Electricity
ACTIVISION BLIZZARD	Leisure Goods
CBS B	Media
FIFTH THIRD BANCORP	Banks
VIACOM B	Media
LABORATORY CORP.OF AM. HDG.	Health Care Equipment and Services
CMS ENERGY	Electricity
AMEREN	Gas, Water and Multiutilities
CINTAS	Support Services
INTERPUBLIC GROUP	Media
14-Feb-2008	
99-th percerntile	
DEERE	Industrial Engineering
EATON	General Industrials
KEYCORP	Banks
95-th percerntile	
BANK OF AMERICA	Banks
DANAHER	General Industrials
TARGET	General Retailers
STRYKER	Health Care Equipment and Services
EMERSON ELECTRIC	Electronic and Electrical Equipment
AVALONBAY COMMNS.	Real Estate Investment Trusts
GENERAL GW.PROPS.	Real Estate Investment Trusts
PACCAR	Industrial Engineering
C R BARD	Health Care Equipment and Services
NORDSTROM	General Retailers
MARTIN MRTA.MATS.	Construction and Materials
NVIDIA	Technology Hardware and Equipment
MACERICH	Real Estate Investment Trusts
04-Sep-2008	

- Continued on next page -

Table 1 – continued from previous page

	99-th percerntile
ALEXION PHARMS.	Pharmaceuticals and Biotechnology
PERRIGO	Pharmaceuticals and Biotechnology
RED HAT	Software and Computer Services
	95-th percerntile
BRISTOL MYERS SQUIBB	Pharmaceuticals and Biotechnology
ELI LILLY	Pharmaceuticals and Biotechnology
STARBUCKS	Travel and Leisure
BROADCOM A	Technology Hardware and Equipment
MYLAN	Pharmaceuticals and Biotechnology
O REILLY AUTOMOTIVE	General Retailers
ROSS STORES	General Retailers
DOLLAR TREE	General Retailers
HORMEL FOODS	Food Producers
LEVEL 3 COMMS.	Fixed Line Telecommunications
CENTURYLINK	Fixed Line Telecommunications
AKAMAI TECHS.	Software and Computer Services
TRACTOR SUPPLY	General Retailers
	02-Oct-2008
	99-th percerntile
STARBUCKS	Travel and Leisure
RED HAT	Software and Computer Services
SANDISK	Technology Hardware and Equipment
	95-th percerntile
TIME WARNER	Media
ALEXION PHARMS.	Pharmaceuticals and Biotechnology
YAHOO	Software and Computer Services
PERRIGO	Pharmaceuticals and Biotechnology
CORNING	Technology Hardware and Equipment
MICRON TECHNOLOGY	Technology Hardware and Equipment
SKYWORKS SOLUTIONS	Technology Hardware and Equipment
LEVEL 3 COMMS.	Fixed Line Telecommunications
MOTOROLA SOLUTIONS	Technology Hardware and Equipment
REGIONS FINL.NEW	Banks
AGILENT TECHS.	Electronic and Electrical Equipment
AKAMAI TECHS.	Software and Computer Services
KEURIG GREEN MOUNTAIN	Beverages
	30-Oct-2008
	99-th percerntile
SOUTHERN	Electricity
PRAXAIR	Chemicals
SL GREEN REALTY	Real Estate Investment Trusts
	95-th percerntile
MCDONALDS	Travel and Leisure
UNITED PARCEL SER.B	Industrial Transportation
NEXTERA ENERGY	Electricity
PUBLIC STORAGE	Real Estate Investment Trusts
ACE	Nonlife Insurance
HEALTH CARE REIT	Real Estate Investment Trusts
NORFOLK SOUTHERN	Industrial Transportation
ST.JUDE MEDICAL	Health Care Equipment and Services
PPL	Electricity
PROLOGIS	Real Estate Investment Trusts
HCP	Real Estate Investment Trusts
PROGRESSIVE OHIO	Nonlife Insurance
EVERSOURCE ENERGY	Electricity
	28-Nov-2008
	99-th percerntile
EXXON MOBIL	Oil and Gas Producers
CHEVRON	Oil and Gas Producers
TARGET	General Retailers
	95-th percerntile
UNITED PARCEL SER.B	Industrial Transportation
CONOCOPHILLIPS	Oil and Gas Producers
NEXTERA ENERGY	Electricity
EMERSON ELECTRIC	Electronic and Electrical Equipment
PRAXAIR	Chemicals
HEALTH CARE REIT	Real Estate Investment Trusts
HCP	Real Estate Investment Trusts
CAMPBELL SOUP	Food Producers
EVERSOURCE ENERGY	Electricity
HESS	Oil and Gas Producers
MARTIN MRTA.MATS.	Construction and Materials
REPUBLIC SVS.A	Support Services
CH ROBINSON WWD.	Industrial Transportation
	08-Apr-2010
	99-th percerntile
PROCTER & GAMBLE	Household Goods and Home Construction
EXELON	Electricity
CENTURYLINK	Fixed Line Telecommunications
	95-th percerntile
3M	General Industrials
UNITED TECHNOLOGIES	Aerospace and Defense

- Continued on next page -

Table 1 – continued from previous page

REYNOLDS AMERICAN	Tobacco
EXPRESS SCRIPTS HOLDING	Health Care Equipment and Services
HEWLETT-PACKARD	Technology Hardware and Equipment
CATERPILLAR	Industrial Engineering
GENERAL DYNAMICS	Aerospace and Defense
AUTOMATIC DATA PROC.	Support Services
CSX	Industrial Transportation
PG&E	Electricity
CUMMINS	Industrial Engineering
QUEST DIAGNOSTICS	Health Care Equipment and Services
BED BATH & BEYOND	Household Goods and Home Construction
06-May-2010	
99-th percerntile	
PROCTER & GAMBLE	Household Goods and Home Construction
3M	General Industrials
CENTURYLINK	Fixed Line Telecommunications
95-th percerntile	
UNITED TECHNOLOGIES	Aerospace and Defense
REYNOLDS AMERICAN	Tobacco
EXPRESS SCRIPTS HOLDING	Health Care Equipment and Services
HEWLETT-PACKARD	Technology Hardware and Equipment
GENERAL DYNAMICS	Aerospace and Defense
AUTOMATIC DATA PROC.	Support Services
JOHNSON CONTROLS	Support Services
CSX	Industrial Transportation
EXELON	Electricity
PG&E	Electricity
TYSON FOODS A	Food Producers
QUEST DIAGNOSTICS	Health Care Equipment and Services
BED BATH & BEYOND	Household Goods and Home Construction
14-Jul-2011	
99-th percerntile	
ANADARKO PETROLEUM	Oil and Gas Producers
EMERSON ELECTRIC	Electronic and Electrical Equipment
SIGMA ALDRICH	Pharmaceuticals and Biotechnology
95-th percerntile	
COCA COLA	Banks
INTERNATIONAL BUS.MCHS.	Software and Computer Services
DANAHER	General Industrials
CATERPILLAR	Industrial Engineering
DEERE	Industrial Engineering
CONSOLIDATED EDISON	Electricity
WEC ENERGY GROUP	Gas, Water and Multiutilities
AMETEK	Electronic and Electrical Equipment
STERICYCLE	Support Services
MACERICH	Real Estate Investment Trusts
FASTENAL	Support Services
DARDEN RESTAURANTS	Travel and Leisure
KEURIG GREEN MOUNTAIN	Beverages
16-Oct-2014	
99-th percerntile	
UNION PACIFIC	Industrial Transportation
ROYAL CARIBBEAN CRUISES	Travel and Leisure
KANSAS CITY SOUTHERN	Industrial Transportation
95-th percerntile	
ALLERGAN	Pharmaceuticals and Biotechnology
THERMO FISHER SCIENTIFIC	Health Care Equipment and Services
EOG RES.	Oil and Gas Producers
HALLIBURTON	Oil Equipment and Services
WILLIAMS	Oil Equipment and Services
AIR PRDS.& CHEMS.	Chemicals
CSX	Industrial Transportation
PPG INDUSTRIES	Chemicals
NORFOLK SOUTHERN	Industrial Transportation
SHERWIN-WILLIAMS	Construction and Materials
PIONEER NTRL.RES.	Oil and Gas Producers
EQT	Oil and Gas Producers
CABOT OIL & GAS A	Oil and Gas Producers

Lists of the firms associated with the most central nodes at given time points.

A Proof of Proposition 1

We start with two preliminary but straightforward lemmas. Throughout, let $\rho_T := Tb_Th_T$ and $\zeta_{n,T} := \min(\rho_T, n)$.

LEMMA A1. *For any $n \in \mathbb{N}_0$,*

$$\sup_{\tau\in\left[\frac{b_T}{2},1-\frac{b_T}{2}\right]} \max_{\ell=1,\ldots,\left\lfloor\frac{1}{h_T}\right\rfloor} \max_{i,j=1,\ldots,n} \left|\widehat{\sigma}^X_{ij;n,T}(\tau,\theta_\ell) - \sigma^X_{ij}(\tau,\theta_\ell)\right| = O_{\mathrm{P}}(\rho_T^{-1/2}) \tag{A1}$$

as $T \to \infty$, with $\theta_\ell = 2\pi h_T \ell$, $\ell = 1, \ldots, \lfloor 1/h_T \rfloor$.

PROOF. The result readily follows from (22) and an application of Chebychev's inequality. □

LEMMA A2. *The eigenvalues $\lambda^X_{j;n}(\tau,\theta)$ of $\mathbf{\Sigma}^X_n(\tau,\theta)$ are such that*

(i) there exist continuous functions $\theta \mapsto \alpha_j(\tau,\theta)$ and $\theta \mapsto \beta_j(\tau,\theta)$, $j = 1, \ldots, q$, and an integer N_X such that, for all $n > N_X$, all $\tau \in [0,1]$, and Lebesgue-a.e. over $\theta \in (0, 2\pi]$,

$$\begin{aligned}\beta_1(\tau,\theta) \geq \frac{\lambda^X_{1;n}(\tau,\theta)}{n} \geq \alpha_1(\tau,\theta) > \beta_2(\tau,\theta) \geq \frac{\lambda^X_{2;n}(\tau,\theta)}{n} \geq \ldots \\ \ldots \geq \alpha_{q-1}(\tau,\theta) > \beta_q(\tau,\theta) \geq \frac{\lambda^X_{q;n}(\tau,\theta)}{n} \geq \alpha_q(\tau,\theta) > 0;\end{aligned} \tag{A2}$$

(ii) there exists a constant B_X such that $\lambda^X_{q+1;n}(\tau,\theta) \leq B_X$ for all $n \in \mathbb{N}$, all $\tau \in [0,1]$ and all $\theta \in (0, 2\pi]$.

PROOF. The result readily follows from Assumptions (C3) and (C4), and an application of Weyl's inequality. □

Turning to the proof of Proposition 1, let us proceed as in the proof of Proposition 7 of Forni et al. (2017). We only highlight here the main steps; details follow along the same lines as in Appendix B (same reference), and are left to the reader.

Lemma A1 implies that, uniformly in $\tau \in [b_T/2, 1 - b_T/2]$ and $\ell = 1, \ldots, \lfloor 1/h_T \rfloor$,

$$\frac{1}{n}\left\|\widehat{\mathbf{\Sigma}}^X_{n,T}(\tau,\theta_\ell) - \mathbf{\Sigma}^X_n(\tau,\theta_\ell)\right\| \leq \frac{1}{n}\sqrt{\sum_{i=1}^n\sum_{j=1}^n \left|\widehat{\sigma}^X_{ij;n,T}(\tau,\theta_\ell) - \sigma^X_{ij}(\tau,\theta_\ell)\right|^2} = O_{\mathrm{P}}(\rho_T^{-1/2}) \tag{A3}$$

as $n, T \to \infty$. Now, for all τ and θ

$$\frac{1}{n}\left\|\widehat{\mathbf{\Sigma}}^X_{n,T}(\tau,\theta) - \mathbf{\Sigma}^\chi_n(\tau,\theta)\right\| \leq \frac{1}{n}\left\|\widehat{\mathbf{\Sigma}}^X_{n,T}(\tau,\theta) - \mathbf{\Sigma}^X_n(\tau,\theta)\right\| + \frac{1}{n}\left\|\mathbf{\Sigma}^\xi_n(\tau,\theta)\right\|,$$

and hence, in view of Assumption (C4),

$$\frac{1}{n}\left\|\widehat{\mathbf{\Sigma}}^X_{n,T}(\tau,\theta_\ell) - \mathbf{\Sigma}^\chi_n(\tau,\theta_\ell)\right\| = O_{\mathrm{P}}(\max(\rho_T^{-1/2}, n^{-1})) \tag{A4}$$

as $n, T \to \infty$ and uniformly in $\tau \in [b_T/2, 1 - b_T/2]$ and $\ell = 1, \ldots, \lfloor 1/h_T \rfloor$.

Let $\mathbf{e}_i$ denote the ith canonical coordinate vector in $\mathbb{R}^n$. From (A3) and (A4), we immediately obtain, uniformly in $\tau \in [b_T/2, 1 - b_T/2]$, $\ell = 1, \ldots, \lfloor 1/h_T \rfloor$ and $i = 1, \ldots, n$,

$$\frac{1}{\sqrt{n}}\left\|\mathbf{e}_i'\left(\widehat{\mathbf{\Sigma}}^X_{n,T}(\tau,\theta_\ell) - \mathbf{\Sigma}^X_n(\tau,\theta_\ell)\right)\right\| = O_{\mathrm{P}}(\rho_T^{-1/2}), \tag{A5}$$

and

$$\frac{1}{\sqrt{n}}\left\|\mathbf{e}_i'\left(\widehat{\mathbf{\Sigma}}^X_{n,T}(\tau,\theta_\ell) - \mathbf{\Sigma}^\chi_n(\tau,\theta_\ell)\right)\right\| = O_{\mathrm{P}}(\zeta_{n,T}^{-1/2}) \tag{A6}$$

as $n, T \to \infty$. This is the analogue of Lemma 1 in Forni et al. (2017).

Next, it follows from (A2) and (A4) that, as $n, T \to \infty$,

$$\begin{aligned}\frac{1}{n}\left|\widehat{\lambda}^{X}_{j;n,T}(\tau,\theta_\ell) - \lambda^{\chi}_{j;n}(\tau,\theta_\ell)\right| &\leq \frac{1}{n}\left\|\widehat{\mathbf{\Sigma}}^{X}_{n,T}(\tau,\theta_\ell) - \mathbf{\Sigma}^{\chi}_{n}(\tau,\theta_\ell)\right\| \\ &= O_{\mathrm{P}}(\max(\rho_T^{-1/2}, n^{-1})) = O_{\mathrm{P}}(\zeta_{n,T}^{-1/2}), \end{aligned} \tag{A7}$$

still uniformly in $\tau \in [b_T/2, 1-b_T/2]$, $\ell = 1, \ldots, \lfloor 1/h_T \rfloor$ and $i = 1, \ldots, n$ (see Lemma 2 in Forni et al., 2017).

Denoting by $\widehat{\mathbf{P}}^{X}_{n,T}(\tau,\theta)$ and $\mathbf{P}^{\chi}_{n}(\tau,\theta)$ the $n \times q$ matrices of leading eigenvectors of $\widehat{\mathbf{\Sigma}}^{X}_{n,T}(\tau,\theta)$ and $\mathbf{\Sigma}^{\chi}_{n}(\tau,\theta)$, respectively, we can show (as in Lemma 3 of Forni et al., 2017) that, uniformly in $\tau \in [b_T/2, 1-b_T/2]$ and $\ell = 1, \ldots, \lfloor 1/h_T \rfloor$,

$$\left\|\widehat{\mathbf{P}}^{X\dagger}_{n,T}(\tau,\theta_\ell)\mathbf{P}^{\chi}_{n}(\tau,\theta_\ell) - \mathbf{W}(\tau,\theta_\ell)\right\| = O_{\mathrm{P}}(\max(\rho_T^{-1/2}, n^{-1})) = O_{\mathrm{P}}(\zeta_{n,T}^{-1/2}). \tag{A8}$$

as $n, T \to \infty$ for some diagonal $q \times q$ matrix $\mathbf{W}(\tau,\theta_\ell)$ the complex diagonal entries of which have modulus one.

Proceeding as in Lemma 4 of Forni et al. (2017), one can show that, denoting by $\widehat{\mathbf{\Lambda}}^{X}_{n,T}(\tau,\theta)$ and $\mathbf{\Lambda}^{\chi}_{n}(\tau,\theta)$ the $q \times q$ diagonal matrices of leading eigenvalues of $\widehat{\mathbf{\Sigma}}^{X}_{n,T}(\tau,\theta)$ and $\mathbf{\Sigma}^{\chi}_{n}(\tau,\theta)$, as $n, T \to \infty$, still uniformly in $\tau \in [b_T/2, 1-b_T/2]$, $\ell = 1, \ldots, \lfloor 1/h_T \rfloor$, and $i = 1, \ldots, n$,

$$\left\|\mathbf{e}_i'\left(\mathbf{P}^{\chi}_{n}(\tau,\theta_\ell)\left[\mathbf{\Lambda}^{\chi}_{n}(\tau,\theta_\ell)\right]^{1/2}\mathbf{W}(\tau,\theta_\ell) - \widehat{\mathbf{P}}^{X}_{n,T}(\tau,\theta_\ell)\left[\widehat{\mathbf{\Lambda}}^{X}_{n,T}(\tau,\theta_\ell)\right]^{1/2}\right)\right\| = O_{\mathrm{P}}(\zeta_{n,T}^{-1/2}). \tag{A9}$$

Recall that the estimator of the spectral density matrix of common components is

$$\widehat{\mathbf{\Sigma}}^{\chi}_{n,T}(\tau,\theta) = \widehat{\mathbf{P}}^{X}_{n,T}(\tau,\theta)\widehat{\mathbf{\Lambda}}^{X}_{n,T}(\tau,\theta)\widehat{\mathbf{P}}^{X\dagger}_{n,T}(\tau,\theta)$$

with (i,j) entry $\widehat{\sigma}^{\chi}_{ij;n,T}(\tau,\theta)$. We then have that, as $n, T \to \infty$,

$$\sup_{\tau \in \left[\frac{b_T}{2}, 1-\frac{b_T}{2}\right]} \max_{\ell=1,\ldots,\left\lfloor \frac{1}{h_T}\right\rfloor} \max_{i,j=1,\ldots,n} |\widehat{\sigma}^{\chi}_{ij;n,T}(\tau,\theta_\ell) - \sigma^{\chi}_{ij}(\tau,\theta_\ell)| = O_{\mathrm{P}}(\zeta_{n,T}^{-1/2}), \tag{A10}$$

which is the analogue of of Proposition 7 in Forni et al. (2017).

The (i,j) entry of the estimated lag k autocovariance matrix $\widehat{\mathbf{\Gamma}}^{\chi}_{n,T}(\tau,k)$ defined in (17) is

$$\widehat{\gamma}^{\chi}_{ij;n,T}(\tau,k) = 2\pi\lfloor h_T \rfloor \sum_{\ell=1}^{\lfloor 1/h_T \rfloor} e^{\iota k\theta_\ell}\widehat{\sigma}^{\chi}_{ij;n,T}(\tau,\theta_\ell); \tag{A11}$$

by definition of a lag k autocovariance, its population counterpart satisfies

$$\gamma^{\chi}_{ij}(\tau,k) = \int_0^{2\pi} e^{\iota k\theta}\sigma^{\chi}_{ij}(\tau,\theta)\mathrm{d}\theta. \tag{A12}$$

Therefore, for any given lag k, we have (letting $\theta_0 := 0$ and $\theta_{\lfloor 1/h_T \rfloor + 1} := 2\pi$)

$$\begin{aligned}
\left|\widehat{\gamma}^{\chi}_{ij;n,T}(\tau,k) - \gamma^{\chi}_{ij}(\tau,k)\right| \leq{}& 2\pi\lfloor h_T\rfloor \sum_{\ell=1}^{\lfloor 1/h_T\rfloor} \left|e^{\iota k\theta_\ell}\widehat{\sigma}^{\chi}_{ij;n,T}(\tau,\theta_\ell) - e^{\iota k\theta_\ell}\sigma^{\chi}_{ij}(\tau,\theta_\ell)\right| \\
&+ \left|2\pi\lfloor h_T\rfloor \sum_{\ell=1}^{\lfloor 1/h_T\rfloor} e^{\iota k\theta_\ell}\sigma^{\chi}_{ij}(\tau,\theta_\ell) - \int_0^{2\pi} e^{\iota k\theta}\sigma^{\chi}_{ij}(\tau,\theta)\mathrm{d}\theta\right| \\
\leq{}& 2\pi\lfloor h_T\rfloor \sum_{\ell=1}^{\lfloor 1/h_T\rfloor} \left|\widehat{\sigma}^{\chi}_{ij;n,T}(\tau,\theta_\ell) - \sigma^{\chi}_{ij}(\tau,\theta_\ell)\right| \\
&+ 2\pi\lfloor h_T\rfloor \sum_{\ell=1}^{\lfloor 1/h_T\rfloor} \max_{\theta_{\ell-1}\leq\theta\leq\theta_\ell} \left|e^{\iota k\theta_\ell}\sigma^{\chi}_{ij}(\tau,\theta_\ell) - e^{\iota k\theta}\sigma^{\chi}_{ij}(\tau,\theta)\right| \\
\leq{}& 2\pi \max_{\ell=1,\ldots,\left\lfloor\frac{1}{h_T}\right\rfloor} \left|\widehat{\sigma}^{\chi}_{ij;n,T}(\tau,\theta_\ell) - \sigma^{\chi}_{ij}(\tau,\theta_\ell)\right| \\
&+ 2\pi\lfloor h_T\rfloor C_2^2 \sum_{\ell=1}^{\lfloor 1/h_T\rfloor} \max_{\theta_{\ell-1}\leq\theta\leq\theta_\ell} \left|e^{\iota k\theta_\ell} - e^{\iota k\theta}\right| \\
&+ 2\pi\lfloor h_T\rfloor \sum_{\ell=1}^{\lfloor 1/h_T\rfloor} \max_{\theta_{\ell-1}\leq\theta\leq\theta_\ell} \left|\sigma^{\chi}_{ij}(\tau,\theta_\ell) - \sigma^{\chi}_{ij}(\tau,\theta)\right| \\
={}& O_{\mathrm{P}}(\zeta_{n,T}^{-1/2}) + O(h_T),
\end{aligned} \tag{A13}$$

where C_2 is the constant in Assumption (B2); (A10) was used to bound the first term, the second one is obviously bounded, and the third one is bounded in view of of Assumption (B).

Now, since (A10) holds uniformly, from (A13) and the fact that $h_T < T^{-1/2}$, by Assumption (F), we have

$$\sup_{\tau\in\left[\frac{b_T}{2},1-\frac{b_T}{2}\right]} \max_{i,j=1,\ldots,n} \left|\widehat{\gamma}^{\chi}_{ij;n,T}(\tau,k) - \gamma^{\chi}_{ij}(\tau,k)\right| = O_{\mathrm{P}}(\zeta_{n,T}^{-1/2}), \tag{A14}$$

which extends Proposition 8 in Forni et al. (2017) to the time-varying case.

We now turn to Part *(ii)* of the estimation procedure (VAR filtering). Assuming that n factorizes, for some integer m, into $m(q+1)$, m distinct $(q+1)$-dimensional VAR models of order at most S (in view of Assumption (D2)) are to be estimated via Yule-Walker. For the sake of simplicity, let us assume $S = 1$: the Yule-Walker estimators of the VAR(1) coefficients (see also (18)) then are

$$\widehat{\mathbf{A}}^{k}_{n,T}(\tau) = \widehat{\mathbf{\Gamma}}^{\chi^k}_{n,T}(\tau,1)\left[\widehat{\mathbf{\Gamma}}^{\chi^k}_{n,T}(\tau,0)\right]^{-1}, \qquad k = 1,\ldots,m.$$

where $\widehat{\mathbf{\Gamma}}^{\chi^k}_{n,T}(\tau,\ell)$ is the $(q+1)\times(q+1)$ sub-matrix of $\widehat{\mathbf{\Gamma}}^{\chi}_{n,T}(\tau,\ell)$ corresponding to the lag ℓ autocovariance matrix of the subvector $\boldsymbol{\chi}^k_{n,T;\tau}$.

Assumption (D4) and the consistency of $\widehat{\mathbf{\Gamma}}^{\chi^k}_{n,T}(\tau,0)$ imply that $\det\widehat{\mathbf{\Gamma}}^{\chi^k}_{n,T}(\tau,0) > d/2$ with probability arbitrarily close to one for T large enough. The same arguments as in Appendix C of Forni et al. (2017) and (A14) then entail, as $n,T\to\infty$,

$$\sup_{\tau\in\left[\frac{b_T}{2},1-\frac{b_T}{2}\right]} \max_{k=1,\ldots,m} \left\|\widehat{\mathbf{A}}^{k}_{n,T}(\tau) - \mathbf{A}^{k}_{n}(\tau)\right\| = O_{\mathrm{P}}(\zeta_{n,T}^{-1/2}), \tag{A15}$$

which extends Proposition 9 in Forni et al. (2017) to the time-varying setting. Moreover, writing $\widehat{\mathbf{A}}_{n,T}(\tau)$ for the $n\times n$ block-diagonal matrix with siagonal blocks $\widehat{\mathbf{A}}^1_{n,T}(\tau),\ldots,\widehat{\mathbf{A}}^m_{n,T}(\tau)$, from

(A15) we have

$$\sup_{\tau\in\left[\frac{b_T}{2},1-\frac{b_T}{2}\right]}\max_{k=1,\ldots,m}\frac{1}{\sqrt{n}}\left\|\widehat{\mathbf{A}}_{n,T}(\tau)-\mathbf{A}_n(\tau)\right\|=O_{\mathrm{P}}(\zeta_{n,T}^{-1/2}),\tag{A16}$$

since $\mathbf{A}_n(\tau)$ has only $m(q+1)^2$ non-zero entries.

We now let $t=\lfloor\tau T\rfloor$ and $\mathcal{T}_T:=\{\lfloor\frac{Tb_T}{2}\rfloor,\ldots,T-\lfloor\frac{Tb_T}{2}\rfloor\}$, and establish the following two lemmas.

Lemma A3. *Under Assumptions (A) and (B),*
(i) $\max_{t\in\mathcal{T}_T}\max_{i=1,\ldots,n}|X_{it}|=O_{\mathrm{P}}(\log^{1/2}T)$*;*
(ii) $\max_{t\in\mathcal{T}_T}\max_{i=1,\ldots,n}|X_{it;t/T}|=O_{\mathrm{P}}(\log^{1/2}T)$.

Proof. First notice that since $\{\mathbf{u}_t\}$ is Gaussian because of Assumption (A1), then for any $\epsilon>0$, there exists an $M>0$ such that (see e.g. Section 2.5. in Vershynin, 2018)

$$\mathrm{P}(\max_{t\in\mathcal{T}_T}\max_{j=1,\ldots,q}|u_{jt}|>\epsilon)\leq Tq\mathrm{P}(|u_{jt}|>\epsilon)\leq 2Tq\exp\left(-\epsilon^2M\right).$$

Hence, $\max_{t\in\mathcal{T}_T}\max_{j=1,\ldots,q}|u_{jt}|=O_{\mathrm{P}}(\log^{1/2}T)$. Likewise, since we assume $n=O(T^\omega)$ for some $\omega>0$, then $\max_{t\in\mathcal{T}_T}\max_{j=1,\ldots,n}|\eta_{jt}|=O_{\mathrm{P}}(\log^{1/2}T)$. The proof then follows from square-summability of the coefficients in (3), (4), (7) and (8) due to Assumptions (B1), (B2), and (B5). □

Lemma A4. *Under Assumptions (A) and (B),*

$$\max_{t\in\mathcal{T}_T}\max_{i=1,\ldots,n}|X_{it}-X_{it;t/T}|=O_{\mathrm{P}}(T^{-1}\log^{1/2}T).$$

Proof. First let us show that

$$\max_{t\in\mathcal{T}_T}\max_{i=1,\ldots,n}|\chi_{it}-\chi_{it;t/T}|=O_{\mathrm{P}}(T^{-1}\log^{1/2}T).\tag{A17}$$

Without loss of generality, let us assume $q=1$: index j and the sums over j then can be dropped. From (3) and (7), for any i and K,

$$\left|\chi_{it}-\chi_{it;t/T}\right|\leq\sum_{k=0}^{K}|c_{ik}^*(t)-c_{ik}(t/T)|\,|u_{t-k}|+\left|\sum_{k=K+1}^{\infty}(c_{ik}^*(t)-c_{ik}(t/T))u_{t-k}\right|.$$

Assumptions (B1) and (B2) imply that, for any $\varepsilon>0$ and $\eta>0$, there exists a $K^*=K(\varepsilon,\eta)$ independent of i, t, and T such that

$$\mathrm{P}\left[\left|\sum_{k=K^*+1}^{\infty}(c_{ik}^*(t)-c_{ik}(t/T))u_{t-k}\right|>\eta/2\right]\leq\varepsilon/2.$$

Hence,

$$\begin{aligned}\mathrm{P}\left[\left|\chi_{it}-\chi_{it;t/T}\right|>\eta\right]&\leq\mathrm{P}\left[\sum_{k=0}^{K^*}|c_{ik}^*(t)-c_{ik}(t/T)|\,|u_{t-k}|>\eta/2\right]\\&\quad+\mathrm{P}\left[\left|\sum_{k=K^*+1}^{\infty}(c_{ik}^*(t)-c_{ik}(t/T))u_{t-k}\right|>\eta/2\right]\\&\leq\mathrm{P}\left[\sum_{k=0}^{K^*}|c_{ik}^*(t)-c_{ik}(t/T)|\,|u_{t-k}|>\eta/2\right]+\varepsilon/2.\end{aligned}\tag{A18}$$

Now, from B4,

$$\mathrm{P}\left[\sum_{k=0}^{K^*}|c_{ik}^*(t)-c_{ik}(t/T)|\,|u_{t-k}|>\eta/2\right]\leq \mathrm{P}\left[\frac{K^*C_4}{T}\max_{1\leq t\leq T}|u_t|>\eta/2\right]$$

where (see the proof of Lemma A3) $\max_{1\leq t\leq T}|u_t|$ is $O_{\mathrm{P}}(\log^{1/2}T)$. It follows that there exists $T^*=T(\varepsilon,\eta)$ independent of i and t such that

$$\mathrm{P}\left[\sum_{k=0}^{K^*}|c_{ik}^*(t)-c_{ik}(t/T)|\,|u_{t-k}|>\eta/2\right]\leq \varepsilon/2 \tag{A19}$$

for all $T\geq T^*$; (A17) follows from putting together (A18) and (A19). The proof of

$$\max_{t\in\mathcal{T}_T}\max_{i=1,\ldots,n}|\xi_{it}-\xi_{i;t/T}|=O_{\mathrm{P}}(T^{-1}\log^{1/2}T)$$

follows along the same steps. The claim follows. □

Proceeding to step *(iii)* of the estimation procedure, letting $t=\lfloor\tau T\rfloor$ and $S=1$ in (19), we obtain

$$\widehat{\mathbf{Z}}_{nt;t/T}:=\left[\mathbf{I}_n-\widehat{\mathbf{A}}_{n,T}(t/T)L\right]\mathbf{X}_{nt},\qquad t\in\mathcal{T}_T:=\{\lfloor\tfrac{Tb_T}{2}\rfloor,\ldots,T-\lfloor\tfrac{Tb_T}{2}\rfloor\}. \tag{A20}$$

Defining

$$\widetilde{\mathbf{Z}}_{nt;t/T}:=\left[\mathbf{I}_n-\mathbf{A}_n(t/T)L\right]\mathbf{X}_{nt},\qquad t\in\mathcal{T}_T, \tag{A21}$$

it follows from (A16) and Lemma A3 that, as $n,T\to\infty$ (note that the filters in (A20) and (A21) just load $(q+1)$ series at a time)

$$\max_{t\in\mathcal{T}_T}\frac{1}{\sqrt{n}}\left\|\widehat{\mathbf{Z}}_{nt;t/T}-\widetilde{\mathbf{Z}}_{nt;t/T}\right\|=O_{\mathrm{P}}(\zeta_{nT}^{-1/2}\log^{1/2}T). \tag{A22}$$

Lemma A4 moreover implies that, as $n,T\to\infty$,

$$\max_{t\in\mathcal{T}_T}\frac{1}{\sqrt{n}}\left\|\widetilde{\mathbf{Z}}_{nt;t/T}-\mathbf{Z}_{nt;t/T}\right\|=O_{\mathrm{P}}(T^{-1}\log^{1/2}T). \tag{A23}$$

Combining (A22) and (A23) yields

$$\max_{t\in\mathcal{T}_T}\frac{1}{\sqrt{n}}\left\|\widehat{\mathbf{Z}}_{nt;t/T}-\mathbf{Z}_{nt;t/T}\right\|=O_{\mathrm{P}}(\zeta_{nT}^{-1/2}\log^{1/2}T) \tag{A24}$$

as $n,T\to\infty$.

Next, consider the rolling covariance matrix for the unobservable $\mathbf{Z}_{nt;t/T}$

$$\widehat{\mathbf{\Gamma}}_n^Z(t/T):=\frac{1}{T}\sum_{s=1}^{T}\mathrm{J}\left(\frac{t-s}{Tb_T}\right)\mathbf{Z}_{ns;t/T}\mathbf{Z}'_{ns;t/T},\quad t\in\mathcal{T}_T. \tag{A25}$$

Then, comparing (20) with (A25),

$$\begin{aligned}\frac{1}{n}\left\|\widehat{\mathbf{\Gamma}}_n^{\hat{Z}}(t/T)-\widehat{\mathbf{\Gamma}}_n^Z(t/T)\right\|&=\frac{1}{nT}\left\|\sum_{s=1}^{T}\mathrm{J}\left(\frac{t-s}{Tb_T}\right)\left[\widehat{\mathbf{Z}}_{ns;t/T}\widehat{\mathbf{Z}}'_{ns;t/T}-\mathbf{Z}_{ns;t/T}\mathbf{Z}'_{ns;t/T}\right]\right\|\\&\leq\frac{1}{nT}\left\|\sum_{s=1}^{T}\left[\widehat{\mathbf{Z}}_{ns;t/T}\widehat{\mathbf{Z}}'_{ns;t/T}-\mathbf{Z}_{ns;t/T}\mathbf{Z}'_{ns;t/T}\right]\right\|\end{aligned} \tag{A26}$$

since $\mathrm{J}(x) \leq 1$ for all $x \in \mathbb{R}$. Now, by generalizing the arguments of Appendix D and especially Lemma 11 in Forni et al. (2017), we can bound, using (A24), the right-hand side of (A26) uniformly over $t \in \mathcal{T}_T$, so that

$$\max_{t\in\mathcal{T}_T} \frac{1}{n} \left\| \widehat{\mathbf{\Gamma}}_n^{\hat{Z}}(t/T) - \widehat{\mathbf{\Gamma}}_n^{Z}(t/T) \right\| = O_{\mathrm{P}}(\zeta_{n,T}^{-1/2} \log^{1/2} T) \tag{A27}$$

as $n, T \to \infty$. Moreover, letting $\mathbf{\Gamma}_n^Z(t/T)$ denote the time-varying covariance matrix of the filtered process $\mathbf{Z}_{n;t/T}$ obtained from $\mathbf{X}_{n;t/T}$ as defined in (6) and (7), from Rodríguez-Poo and Linton (2001, Proposition 3.2) and Motta et al. (2011, Theorem 1), we have (since $(Tb_T)^{-1/2}$ is dominated by $(Tb_Th_T)^{-1/2}$)

$$\max_{t\in\mathcal{T}_T} \frac{1}{n} \left\| \widehat{\mathbf{\Gamma}}_n^{Z}(t/T) - \mathbf{\Gamma}_n^{Z}(t/T) \right\| = O_{\mathrm{P}}((b_TT)^{-1/2}) = O_{\mathrm{P}}(\rho_T^{-1/2}) \tag{A28}$$

as $n, T \to \infty$.

Now, by Assumption (A1) we have $\mathrm{E}[\mathbf{u}_t\mathbf{u}_t'] = \mathbf{I}_q$, therefore for all $\tau \in [0,1]$ the common component of the static factor model (14) has covariance $\mathbf{\Gamma}_n^{\psi}(\tau) = \mathbf{R}_n(\tau)\mathbf{R}_n'(\tau)$ and by construction we have $\mathbf{R}_n(\tau) := \mathbf{V}_n^{\psi}(\tau)[\mathbf{M}^{\psi}(\tau)]^{1/2}$, where $\mathbf{M}^{\psi}(\tau)$ is the $q \times q$ diagonal matrix with the q largest eigenvalues of $\mathbf{\Gamma}_n^{\psi}(\tau)$ and $\mathbf{V}_n^{\psi}(\tau)$ the $n \times q$ matrix of the corresponding normalized eigenvectors. Following the same arguments as in Proposition 10 in Forni et al. (2017), starting from of (A27) and (A28) we obtain, as $n, T \to \infty$,

$$\max_{t\in\mathcal{T}_T} \frac{1}{n} \left\| \widehat{\mathbf{M}}^{\hat{Z}}(t/T) - \mathbf{M}^{\psi}(t/T) \right\| = O_{\mathrm{P}}(\zeta_{n,T}^{-1/2} \log^{1/2} T),$$

and

$$\max_{t\in\mathcal{T}_T} \left\| \widehat{\mathbf{V}}^{\hat{Z}}(t/T) - \mathbf{V}^{\psi}(t/T) \right\| = O_{\mathrm{P}}(\zeta_{n,T}^{-1/2} \log^{1/2} T).$$

Therefore, since, by definition, $\widehat{\mathbf{R}}_n(t/T) := \widehat{\mathbf{V}}_n^{\hat{Z}}(t/T)[\widehat{\mathbf{M}}^{\hat{Z}}(t/T)]^{1/2}$, we have

$$\max_{t\in\mathcal{T}_T} \frac{1}{\sqrt{n}} \left\| \widehat{\mathbf{R}}_n(t/T) - \mathbf{R}_n(t/T)\mathbf{S}(t/T) \right\| = O_{\mathrm{P}}(\zeta_{n,T}^{-1/2} \log^{1/2} T), \tag{A29}$$

still as $n, T \to \infty$, where $\mathbf{S}(t/T)$ is a $q \times q$ diagonal matrix with entries ± 1. By combining (A15) and (A29), and in view of (the definition of impulse response functions)

$$\widehat{\mathbf{C}}_{n,T}^{*}(t, L) := [\widehat{\mathbf{A}}_{n,T}(t/T, L)]^{-1}\widehat{\mathbf{R}}_{n,T}(t/T), \qquad \mathbf{C}_n(t/T, L) := [\mathbf{A}_n(t/T, L)]^{-1}\mathbf{R}_n(t/T),$$

for any given $k \geq 0$, as $n, T \to \infty$, we have

$$\max_{t\in\mathcal{T}_T} \max_{\substack{i=1,\dots,n \\ j=1,\dots,q}} \left| \widehat{c}_{ijk;n,T}^{*}(t) - s_j(t)c_{ijk}(t/T) \right| = O_{\mathrm{P}}(\zeta_{n,T}^{-1/2} \log^{1/2} T). \tag{A30}$$

Moreover, from Assumption (B4), for any given $k \geq 0$, as $T \to \infty$,

$$\max_{t\in\mathcal{T}_T} \max_{\substack{i=1,\dots,n \\ j=1,\dots,q}} \left| c_{ijk}^{*}(t) - c_{ijk}(t/T) \right| = O(T^{-1}). \tag{A31}$$

Combining (A30) and (A31) completes the proof. □

B Additional empirical results

Figure B12: Idiosyncratic components zero-frequency coherence at selected dates

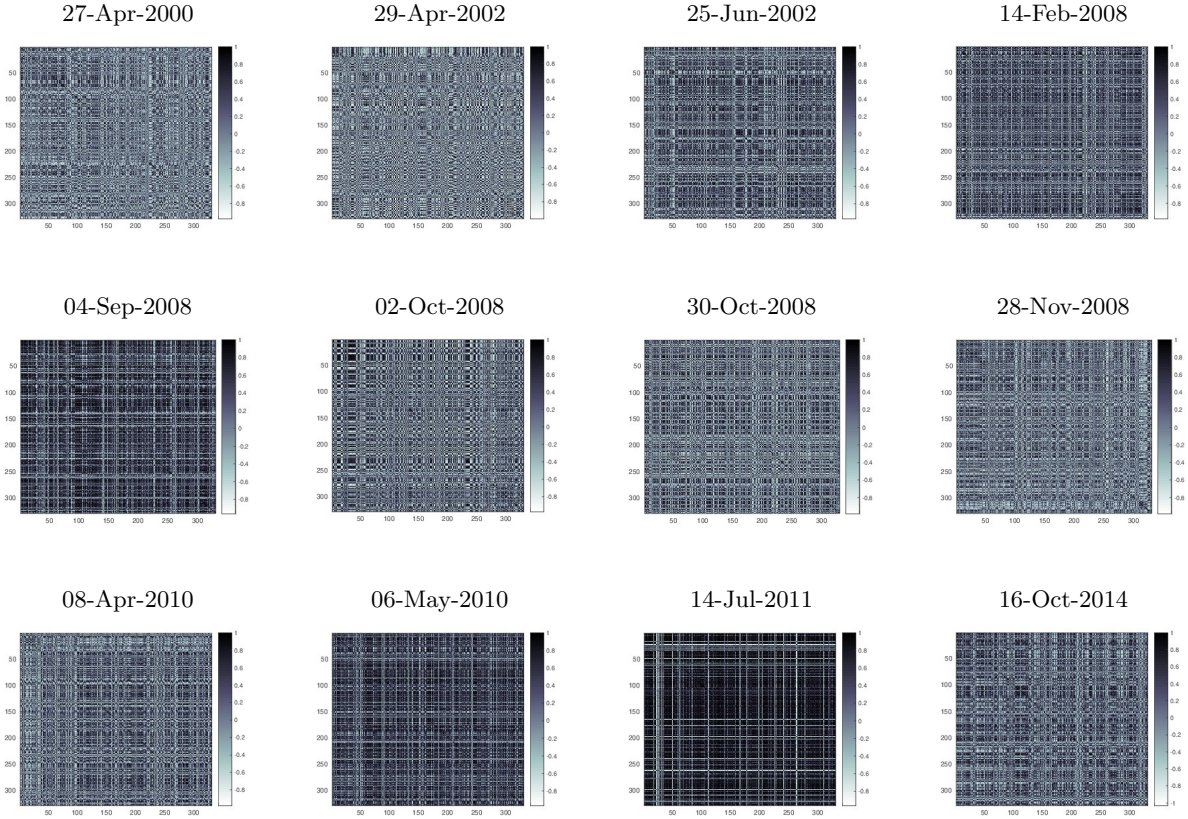

Heatmaps, at selected dates, of the time-varying zero-frequency spectral coherence matrix of the estimated idiosyncratic components, with generic entry $\left|\widehat{\sigma}^{\xi}_{ij;n,T}(t,0)\right|^2/\widehat{\sigma}^{\xi}_{ii;n,T}(t,0)\widehat{\sigma}^{\xi}_{jj;n,T}(t,0)$, $i,j=1,\ldots,n$.

Figure B13: Common components zero-frequency coherence at selected dates

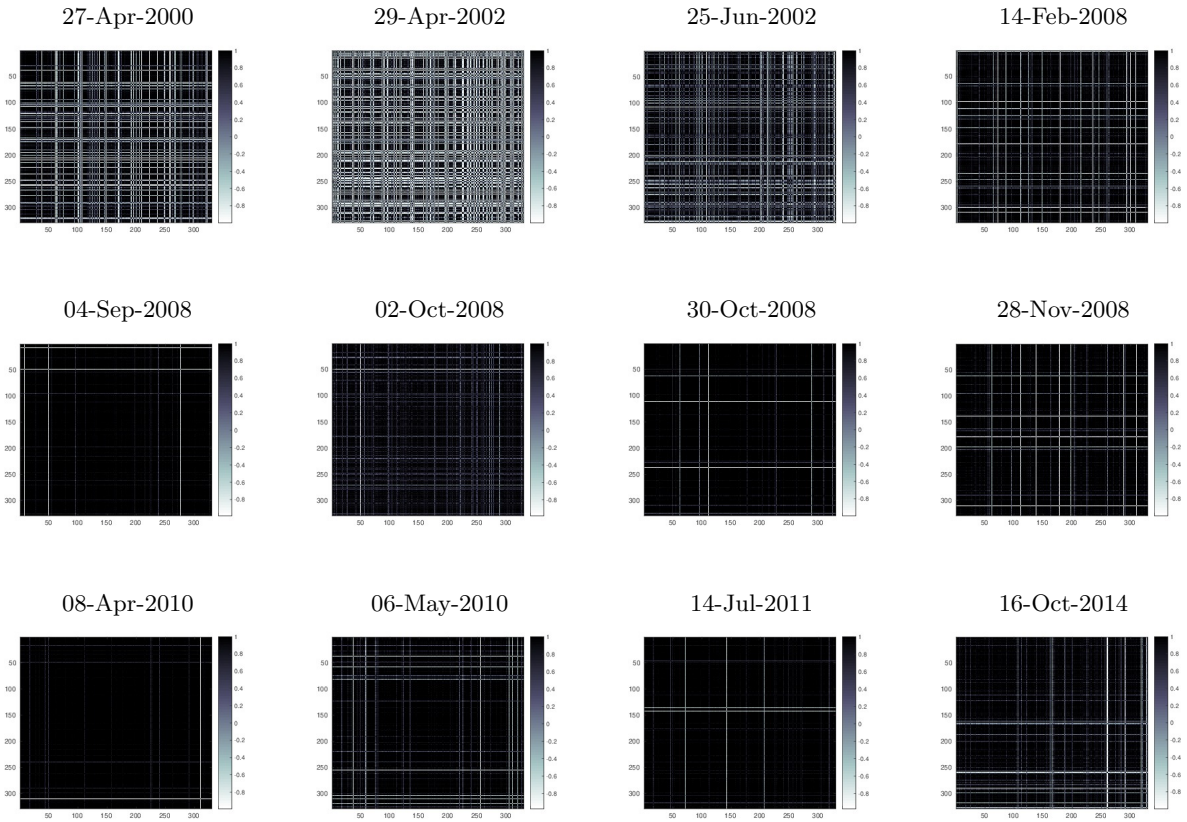

Heatmaps, at selected dates, of the time-varying zero-frequency spectral coherence matrix of the estimated common components, with generic entry $\left|\widehat{\sigma}^{\chi}_{ij;n,T}(t,0)\right|^2/\widehat{\sigma}^{\chi}_{ii;n,T}(t,0)\widehat{\sigma}^{\chi}_{jj;n,T}(t,0)$, $i,j=1,\ldots,n$.

Figure B14: Time-varying eigenvector centrality in long-run connectedness

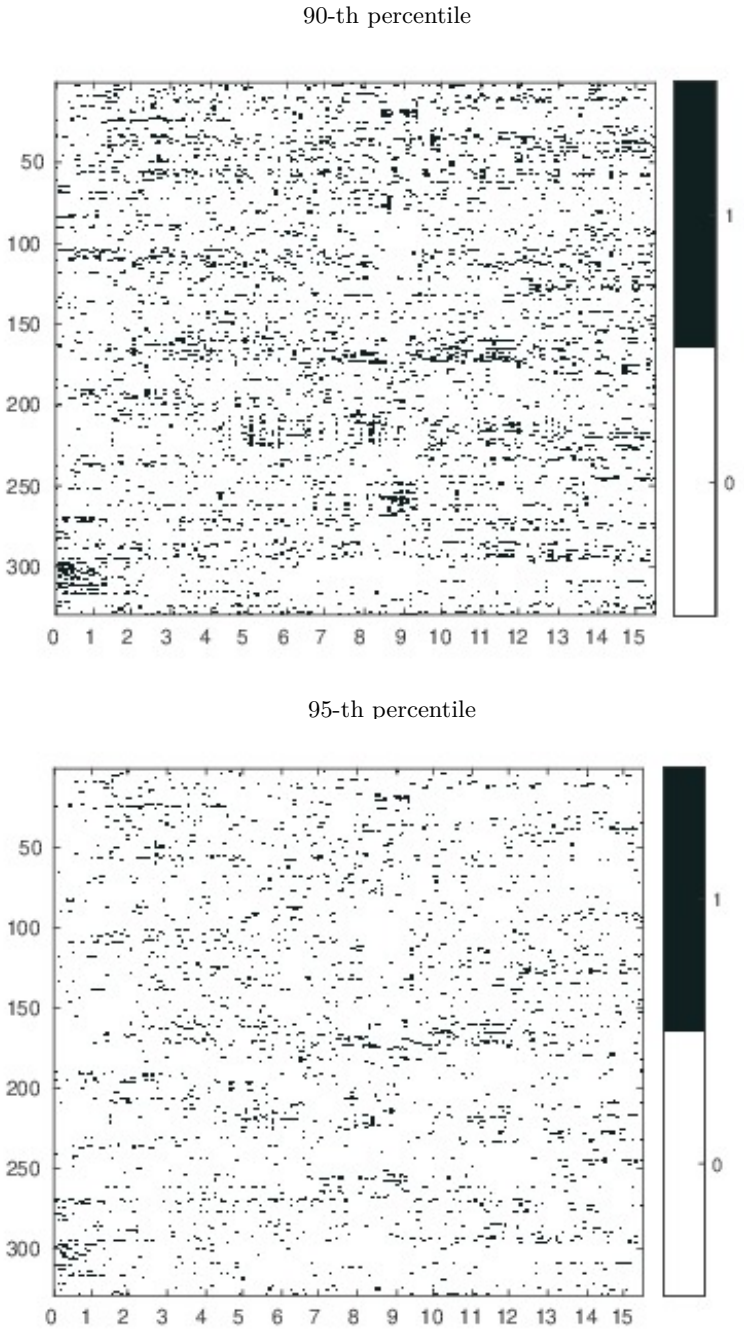

Top panel: $n \times T$-dimensional heatmaps of eigenvector centrality in long-run connectedness; dark cells indicate that, at the date in abscissa, the corresponding firm is above the 90-th percentile of the long-run connectedness eigenvector centrality distribution. Bottom panel: $n \times T$-dimensional heatmaps of eigenvector centrality in long-run connectedness; dark cells indicate that, at the date in abscissa, the corresponding firm is above the 95-th percentile of the long-run connectedness eigenvector centrality distribution.